EXPERIMENTAL MEASURE AND MODELING OF CLAY CATION EXCHANGE CAPACITY AND EVALUATION OF RESERVOIR DEWATERING

A Thesis

by

SEBASTIAN F. SMITH

Submitted to the Office of Graduate and Professional Studies of
Texas A&M University
in partial fulfillment of the requirements for the degree of

MASTER OF SCIENCE

Chair of Committee,	Thomas E. Yancey
Committee Members,	Mukul R. Bhatia
	Berna Hascakir
	Franco Marcantonio
Head of Department,	Julie Newman

May 2020

Major Subject: Geology

Copyright 2019 Sebastian F. Smith

ABSTRACT

This study investigates the relative influences of rock properties (porosity, clay content, grain density, and water saturation) on sediment dewatering in the interests of improving understanding of soaking enhanced oil recovery. In addition to this, the applicability of sample grinding corrections developed for cation exchange capacity (CEC) in sandstones is investigated for application on mudstones and modeling of CEC from XRF data. Investigation of core analysis data (crushed shale analysis, X-ray diffraction (XRD), X-ray fluorescence (XRF), and organic pyrolysis data), and Monte Carlo evaluation of petrophysical equations of pore water storage show the largest changes in calculated desiccation index (DI) are due to variation total clay content and porosity. Changes in grain density and water saturation did not introduce as large a change. Investigation of pyrolysis data shows a relation between high organic richness and higher degrees of desiccation. The relation between organic content and increase in desiccation value is further suggested by the statistical association between redox elements (example: As, Ni, U, Mo) and DI. This study documents a clear linear increase in clay mineral surface area with increasing duration of sample grinding as shown by the corresponding absorption of cobalt hexamine trichloride and the corresponding increase of exchangeable cations (Ca, Na, Mg, K, and Al) in the decanted solution. This study demonstrates the effective application of the Huff (1987) method on mudstones. Inductively coupled mass spectrometry (ICP-MS) presents a relatively inexpensive and time-effective means of quantitatively measuring CEC. Regression modeling of CEC via XRF increases the density of accurate clay property estimations.

DEDICATION

I dedicate this to my parents Scott and Karen Smith for their unceasing love and support, and inspiring me to reach higher and work harder for my dreams. Thank you for being the role models of my life.

ACKNOWLEDGEMENTS

I thank my committee for their astute advice and guidance over the course of my research. I thank Dr. Thomas Yancey for supporting my admission into the Texas A&M University Geology masters program, providing a wealth of geological wisdom, and great help in improving my science communication skills. I thank Dr. Mukul Bhatia for his professional guidance and support in attaining an industry connection for my research. I thanks Dr. Franco Marcantonio for his lab support and guidance with the use of inductively coupled mass spectrometry. I also thank Dr. Berna Hascakir for her time and being my out of department committee member.

I thank my friends that have supported me professionally and emotionally along the way, I could not have done this without you all. I give a big thank you to my housemates Matthew Couchman, and John Greene for their advice and support over the odyssey that has been my degree, glad to have you guys. I thank Dr. Jie Zhao for his enthusiastic support over my two internships with Core Laboratories and inspiring me to research enthusiastically. As well I thank Dr. Craig Hall for his patience in helping guide my research and working though a few rough presentations. I thank Dr. Mamdouh Shebl for his help and support in founding my research, as well as life and professional advice. I give an extra special thank you to Lianna Hall for her enthusiastic love, support and patience as I completed my work. She was the extra boost and inspiration to push me through the finish line. I give huge thanks to my parents for their love and support over the course of my undergraduate and masters study, I could not have done half of this without you two. You inspired the grit that has carried me through these wildfires. I also extend a thank you to Mei Mei for her expert writing advice.

CONTRIBUTORS AND FUNDING SOURCES

Graduate study was supported through the Texas A&M University Berg-Hughes center by a fellowship from BP Energy Company for Fall 2018-Spring 2019, and The Dan A. Hughes' 51 Chair Fellowship Fall 2019. Core data for the research was supplied by Core Laboratories Integrated Reservoir Solutions Houston. Samples for measured cation exchange capacity lab-work were supplied by The Clay Mineral Society. Lab work was completed in the labs of Dr. Franco Marcantonio. Samples were run through the ICP-MS by Ms. Luz Romero.

TABLE OF CONTENTS

Page

LIST OF FIGURES

Page

LIST OF TABLES

Page

LIST OF EQUATIONS

CHAPTER I

INTRODUCTION

Unconventional tight reservoirs make up the backbone of North American land hydrocarbon production. In the United States alone, most new production is sourced from tight formations such as the Bakken, Eagleford, and Marcellus (Yu et al., 2016). Although hydrocarbon production from wells in these formations is initially high, production curves decline rapidly on account of extremely low porosity of these stratigraphic units (Alvarez et al., 2017; Yu et al., 2016). For this reason, an unfortunate companion of unconventional work is drilling for the sake of maintaining production. Consequently, enhancements to the recovery process must be made to improve the economics of wells in unconventional tight reservoirs (Alvarez et al., 2017; Yu et al., 2016). Soaking is one such enhanced oil recovery (EOR) method that plays off natural sub-surface desiccation (reduction of water saturation). It is potentially vital in increasing the lifetime of wells in unconventional tight reservoirs, however, the dynamics of why this process works or conversely, why it does not work, are still under debate.

Soaking is a post-hydraulic fracturing procedure where the result is the rehydration of the rock and the lengthening of the desiccation process. Desiccation is the reduction of water chemically bound to clay mineral surfaces and bound to pore walls by capillary forces. The scientific community has been aware of naturally occurring subsurface desiccation since the

early 1960s. Engelder et al. (2014) compiled many proposed ideas for desiccation into an idealized three-step model:

1. Organic and inorganic rock constituents are deposited, and compacted with burial; 75% or more of initial water content is lost in this step (Burst, 1976).
2. As the kerogen in the rock is cooked, it is converted into hydrocarbons, which enter the matrix and pore space, increasing pressure. Co-occurring with this is this mineral diagenesis, where minerals in the rock are converted to more stable configurations with less surface area, reducing the capacity of the rock to bind water.
3. Increased pressure first displaces all water bound to the capillary space and then strips water chemically bound to the surface of clay minerals. Soaking theoretically lengthens this process by replacing displaced water, thus promoting the production of additional hydrocarbons.

Historically, soaking research has focused on reservoir rocks with higher porosity and lower clay content such as clay-poor sandstones and has been shown to improve production in those rocks (Chakraborty et al., 2015). Despite these successful instances, the application of soaking in mudstone reservoirs has had limited success and is largely characterized as guesswork. Recent studies have expanded the investigation of the effect of soaking on productivity into mudrocks; however, these investigations have attained very different conclusions about the procedure's potential benefit (Bostrom et al., 2014; Dutta et al., 2014; Chakraborty et al., 2015; Lan et al., 2014).

The results of soaking are mixed, even within the same field (Yaich et al., 2015; Lan et al., 2014). Yaich et al. (2015), in their study of the Marcellus, four localities were investigated; soaking was found beneficial to production in three and did not affect the last. Where soaking was applicable, higher initial hydrocarbon flow back after the soaking period was noted in

addition to enhanced production for significant periods (Yaich et al., 2015). Soaking can be associated with decreased water production. However, clay-water interaction responsible for the decrease in water production is also cited as a potential hazard to rock permeability on account of clay swelling as they absorb injected fluids (Yaich et al., 2015). Organic content also affects the ability of rocks to imbibe water. Lan et al. (2014) show a negative association between organic content and water imbibition. In their study Engelder et al. (2014), show that varying organic and clay content affects the volume and rate by which geologic formations absorb water. Sediment dewatering/fluid absorption is affected by whole-rock composition.

This study focuses primarily on the role of porosity, organic content, mineralogy, and clay mineral properties in desiccation. These properties and their relative influence on the final calculated reservoir desiccation value are investigated with data science analysis of x-ray diffraction (XRD), x-ray fluorescence (XRF), and crushed shale analysis data provided by Core Laboratories.

Cation exchange capacity (CEC) is a surface area dependent property of clays and organics that pertains to their ability to exchange cations with the surrounding fluid; a critical factor to known when determining fluid saturations and distributions in the pore space. Clay mineral surfaces have a negative negatively charged “electric double layer,” (Dessouki et al., 2016). This charge imbalance attracts cations in the surrounding fluid and binds them to the clay surface via van der walls force (Dixon and Schulze, 2002). Consequently, CEC is important in the determination of water saturation made up of clay bound water (Bush and Jenkins, 1977). Because of the time, difficulty and errors involved in the direct measure of CEC, numerous methods for the calculation of CEC from resistivity well-logs, and XRD, and XRF have been proposed (Bush and Jenkins, 1977; Huff 1987). The most common method for direct

measurement of CEC is by wet chemistry. This involves sample disaggregation and placement in a solution. The quantity of the solution absorbed permits the determination of sample CEC as the saturating solution binds to available sample surface area, forcing exchangeable cations into solution. In soil science, where the material in question is unconsolidated, disaggregation is a non-issue. However, disaggregation produces additional surface area as sample particle sizes are reduced, resulting in a CEC value larger than the sample would produce in its original unground state. Ignoring contribution by organics, the overall CEC of rock is dependent on the total surface area of clay minerals exposed to porosity. Huff (1987) developed a workflow for correcting this issue for clay poor sandstones, but there is no published workflow for mudrocks. This study applies the Huff (1987) sample grinding method to clay samples to investigate its applicability in mudrocks. In the interests of both time and accuracy in testing, cobalt hexamine trichloride ($[Co(NH_3)6]Cl_3$) was chosen, as it may permit reliable measurement of exchangeable cations from a single extraction, avoiding multiplying of errors that occur with multiple extractions (Ciesielski et al., 1997). Inductively coupled mass spectrometry (ICP-MS) is used for the measurement of exchangeable cations due to the small sample sizes required, relatively low cost of operation, and the speed that large batches of samples may be processed.

This study investigates the controls of unconventional reservoir desiccation and the role of clays in the sediment dewatering model described in Engelder et al. (2014). Sediment dewatering is dependent on total porosity, total clay content, organic properties, total organic matter, and organic properties. CEC is simply the ability of a material to exchange ions (atoms or molecules with a non-zero net charge) with the fluid around it. This term is a critical factor in the determination of clay bound water (Klein, 1979; Juhasz, 1986). Although numerous models exist for estimation of CEC, a precise determination is currently limited to costly and time-consuming

lab-based measurements. This work develops a method for the quick and inexpensive means for determining CEC values for large sample sets.

CHAPTER 2

METHODS

XRD, XRF, organic pyrolysis, and crushed shale analysis data are used in the statistical analysis of sediment dewatering controls. XRD data were collected following the powder method using a Siemens D5000 XRD unit. XRF data was collected using a Thermo Scientific Niton XL3 GOLDD + XRF Analyzer at 0.5 – 1-foot intervals along oil-well rock cores within a standard core-viewing room at room temperature at Core Laboratories, Houston facilities. Collected XRF data were calibrated against known composition standards. Organic pyrolysis data was collected using a RockEval Pyrolysis unit. This unit measures total organic content and organic richness/character by heating samples and vaporizing the organic content. The hydrocarbons produced from this process are used to calculate organic richness, thermal maturity, and kerogen characteristics. Crushed shale analysis data were collected following the Gas Research Institute method (GRI final report: GRI-95/0496). In crushed shale analysis, samples are pulverized to 0.5-0.85mm diameter particles, this eliminates induced fractures and provides means of measuring porosity, permeability, grain density, and gas/fluid saturation of fine-grained rocks.

Clay minerals used for standards in the process of obtaining CEC measurements were obtained from The Clay Mineral Society. Standards include Chlorite (variety Ripidolite), from Flagstaff Hill El Dorado County, California, United States, Kaolinite from Warren County, Georgia, United States, Ca-montmorillonite from Gonzales County, Texas, United States, and Illite from Silver Hill, Montana, United States. Cation exchange capacity work was completed at Texas A&M University via the following methodology:

1. Source clay samples from the Clay Mineral Society (Table 4) were weighed on a Mettler AC100 scale and mixed into combinations of varying weight percentages to represent endmember mud rock compositions (Table 1).

2. Following Huff, (1987): each sample was then split into four sub-samples of equal mass. Three of the sub-samples are then ground for varying lengths of time using a SPEX 8000 Mixer/Mill and then poured into their own test tube. Samples were ground in 30-second increments up to a total of two minutes (Table 2).

3. CEC measurements and cation selectivity are obtained for the samples by equilibrating the powdered samples with cobalt hexamine trichloride for 30 min at room temperature with a solution to solid mass ratio of 30 (Bernard et al., 2018; Ciesielski et al., 1997; Jenni et al., 2014). Samples used in the equilibration experiment are approximately 100 milligrams each and equilibrated with 3 grams of a 0.016 molar cobalt hexamine solution. The fluid from the powder- cobalt hexamine solution was then leached and measured via ICP-MS for concentrations of Na, K, Ca, Mg, Al, and Co to measure ion selectivity and calculation of CEC (Bernard et al., 2018; Ciesielski et al., 1997; Jenni et al., 2014). All ICP-MS tested solutions were measured to 2mL, acidified with 14 microliters of 70% nitric acid to negate sample sticking within the spectrometer, spiked with 100 microliters of 10ppb indium, and diluted 5x in 2% nitric acid to reduce ion concentrations to levels safe for use in the ThermoScientific XR ICP-MS unit. Sample grinding was corrected for following Huff, (1987) method.

	Weight Percent			
Sample	**Illite**	**Smectite**	**Chlorite**	**Kaolinite**
1	100	0	0	0
2	0	100	0	0
3	0	0	100	0
4	25	25	25	25
5	0	0	0	100
6	27	24	24	25

Table 1: Tested samples and their measured mineral weight percentages.

Sample	**Total Grind Time**
1 (Montmorillonite)	1.5 minutes
2 (Kaolinite)	1.5 minutes
3 (Illite)	2 minutes
4 (Chlorite)	2 minutes
5 (27/24/24/25)	2 minutes

Table 2: Tested samples and their total grinding times.

CHAPTER 3

DISCUSSION

The degree of desiccation in a rock can be shown with the desiccation index (DI) (Equation 1). It describes the distribution of water in the rock and quantifies the relative abundance of water bound to clays compared to all other water present. If DI is equal to one, at parity, clay bound water is equivalent to non-clay bound water. If DI is greater than one, the rock is hydrated, with capillary being most of the water bound in the pore spaces. If DI is less than one, the rock is desiccated; water bound to clays represents a majority percentage of water in the pore space.

$$\boldsymbol{DI = \frac{Bulk\ volume\ water\ (BVW)}{Water\ potentially\ bound\ to\ clays\ (CBW)}}$$

Equation 1: Desiccation index, quantification of degree of reservoir dewatering.

Bulk volume water (BVW) (Equation 2) is used to quantify all water in the pore space; it represents the water in the pore space as a percent volume. The values input into the equation (Φ_T and S_W) are measured from crushed shale analysis. Φ_T is the percent volume of the pore space comprised of porosity, and S_W is the percentage of fluid in the rock that is water.

$$\boldsymbol{BVW = \Phi_T\ (\%) \cdot \frac{S_W\ (\%)}{100}}$$

Equation 2: Bulk volume water; statement of all water filling the pore space, no regard to the location of water (i.e. bound to clays). S_W: Total water saturation.

Clay bound water (CBW) (Equation 3) is the volume of water potentially bound to clay minerals. XRD provides the data for determination of the composition of clays in the rock, this is used with average clay CEC values to estimate a maximum potential clay bound water volume.

Grain density and total porosity are measured from crushed shale analysis. Pore fluid salinity is averaged from a high and low estimated value which may not be representative of pore composition. CEC values used are taken from the literature (example see table 3) and may not accurately represent the actual exchange potential. The exchange potential of the rock may vary depending on actual pore fluid salinity, pH, and temperature, affecting the maximum water-binding potential of the rock.

	Formula:	CEC P50, CEC Range (meq^2/g)	Specific Surface $\left(\frac{m^2}{g}\right)$
Smectite Group:	$A_{0.3}D_{2\text{-}3}[T_4O_{10}]Z_2 \cdot nH_2O$ A: Ca, Na, Li, Zn, Mg D: Mg, Al, Li, Fe T: Si, Al Z: F, OH	115, 80-150 (Martin & J. Dacy, 2004) 82 (montmorillonite) (S´anchez-Mart´ın et al., 2007)	750 (montmorillonite) (S´anchez-Mart´ın et al., 2007)
Illite:	$K_{0.65}Al_{2.0}[Al_{0.65}Si_{3.35}O_{10}](OH)_2$	25,10-40 (Martin & J. Dacy, 2004) 15 (S´anchez-Mart´ın et al., 2007)	57 (S´anchez-Mart´ın et al., 2007)
Kaolinite:	$Al_2(Si_2O_5)(OH)_4$	5.5, 1-10 (Martin & J. Dacy, 2004) 6.1 (S´anchez-Mart´ın et al., 2007)	12 (S´anchez-Mart´ın et al., 2007)
Chlorite:	$A_{5\text{-}6}T_4Z_{18}$ A = Al, Fe^{2+}, Fe^{3+}, Li, Mg, Mn, or Ni T = Al, Fe^{3+}, Si or a combination Z = O and/or OH	3, <10 (Martin & J. Dacy, 2004) 1.9 – 14.4 (Cerepi, 2000)	1.7 – 39.5 (Cerepi, 2000)

Table 3: General clay mineral formulas from mindat.org, P50 (average) and range of clay CEC values, and their reported specific surface areas.

$$\boldsymbol{CBW = \Phi_T * (0.6425 * \left(pore\ fluid\ salinity \left(\frac{g}{l}\right)^{-0.5} + 0.22 \right) * \frac{(CEC * (1 - \Phi_T) * \rho_{grain})}{100 * \Phi_T}}$$

Equation 3: Clay bound water; statement of water potentially bound to clays (Klein, 1979; Juhasz, 1986). Φ_T: Total porosity, ρ_{grain}: grain density.

XRD data is used to calculate CEC (Equation 4) for the determination of CBW. The constraints of this equation are the XRD measured weight percent of present clay species and average CEC values from published sources. The goal of this study is to present a more accurate means of inferring reasonable CEC values. Clay minerals may have very different compositions that respond differently to subsurface conditions, this variance is demonstrated by the correlation and covariance of elements associated with calculated CEC (Figure 1, Figure 2). Using published values for CEC assumes homogenous composition and morphology of clay minerals and equivalent response to subsurface conditions. If this assumption was enough, correlation of CEC to elemental data should suggest overwhelming correlation for a few elements as all mineral structures are the same and therefore give preference to certain elements. However, statistically some elements have a greater association than others, we cannot say where they come from in the rock. This is complicated further when many redox elements (example: As, Ni, U, Mo) have an equal association with ions associated with clay mineral structures. Redox elements may vary based on kerogen type and secondary catagenic processes. It is insufficient to assume XRD weight percentages and published CEC values are enough for accurate characterization of clay content properties, measurement of CEC and understanding of clay response to varying pore conditions is necessary to accurately infer subsurface CEC.

$$\boldsymbol{CEC_{XRD} = CEC_{Illite} + CEC_{Kaolinite} + CEC_{Chlorite} + CEC_{Smectite}}$$

Equation 4: Parent statement for XRD calculated CEC, summation of all CEC contributed by individual clay mineral species, equations for individual clay species in appendix (Dacy and Martin, 2004).

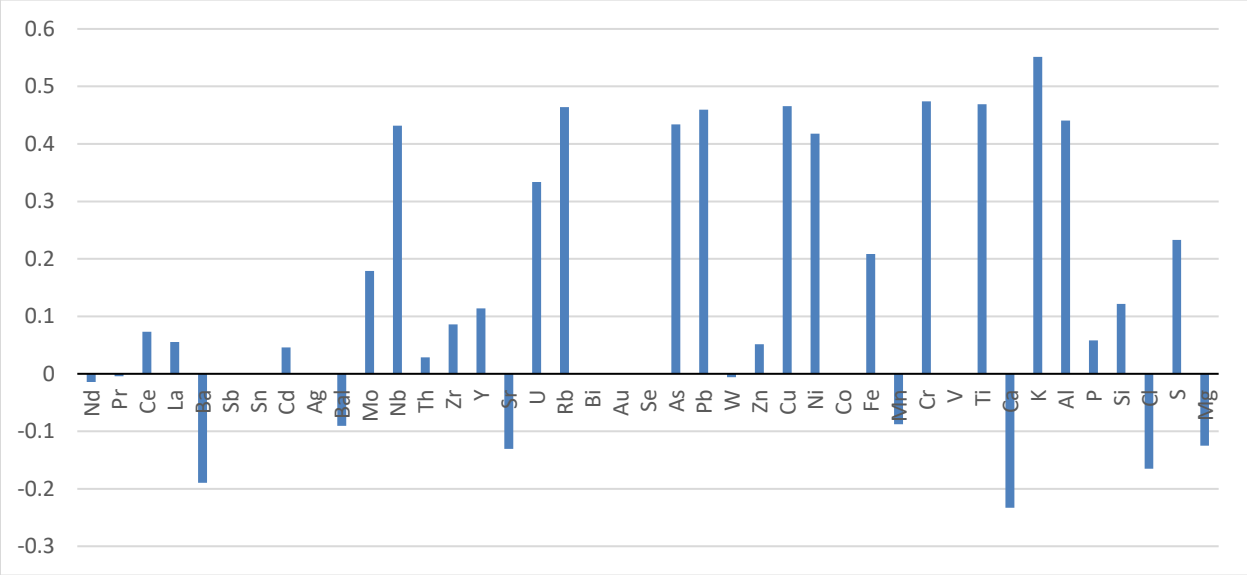

Figure 1: Elements measured by XRF correlation to XRD calculated CEC results. Bars represent calculated correlation of XRD calculated CEC to the element listen underneath.

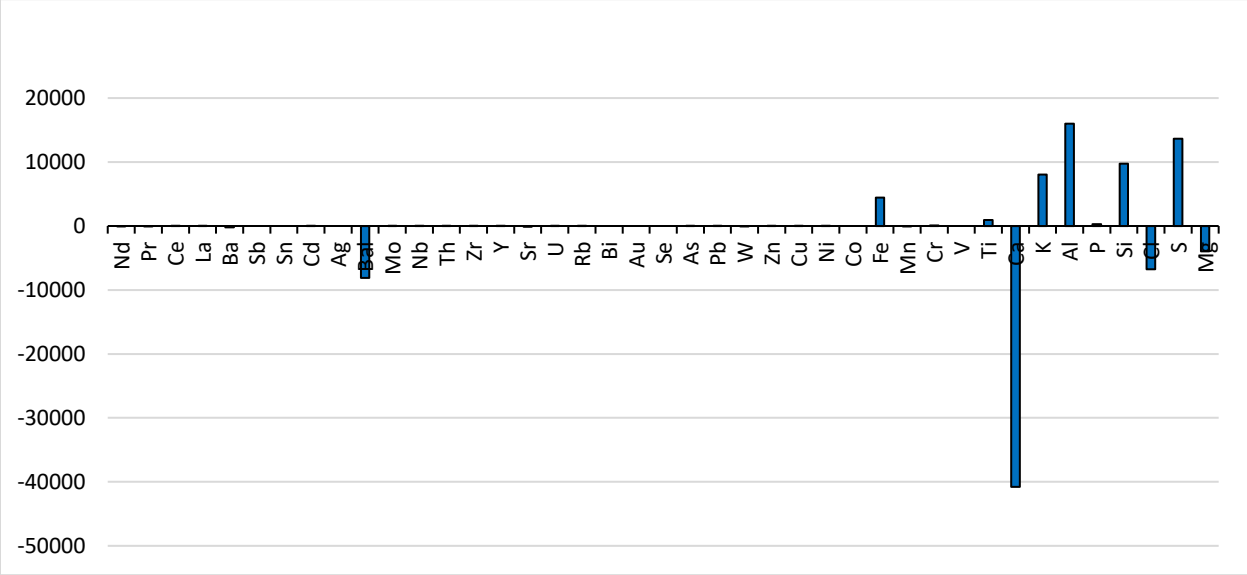

Figure 2: Elements measured by XRF covariance to XRD calculated CEC results. Bars represent calculated covariance of XRD calculated CEC to the element listen underneath.

The bulk of the dataset for characterization of desiccation influences is XRF data. XRF data is only semi-quantitative and must be taken with a grain of salt by itself. However, when statistically compared to a quantitative measure, qualified statements may be made regarding the data. This study satisfies this by looking at the correlation and covariance of XRF element data to crushed shale analysis results, XRD data. As well as CEC, BVW, CBW and DI values derived from crushed shale and XRD. The primary use of the XRF data is to identify elements commonly associated with clay mineral structures (Table 3) for the analysis of elemental association with BVW, CBW, and DI. It is also used to the analysis of the relative association of organic content with BVW, CBW, and DI by looking at redox elements potentially associated with organics. In the investigation of CEC, XRF data is used to identify the elements likely bound to the surface of the clay minerals; exchangeable cations (example K, Na, Ca, Mg). Exchangeable cations provide a picture of the pore fluid composition. Correlation (Equation 9) quantifies the predictive statistical relationship between two independent variables.

$$\boldsymbol{Correlation\ coefficent} = \frac{\sum(\boldsymbol{x} - \underline{\boldsymbol{x}})(\boldsymbol{y} - \underline{\boldsymbol{y}})}{\sqrt{\sum(\boldsymbol{x} - \underline{\boldsymbol{x}})^2 \sum(\boldsymbol{y} - \underline{\boldsymbol{y}})^2}}$$

Equation 5: Formula for correlation coefficient, $\underline{\boldsymbol{x}}$ *and* $\underline{\boldsymbol{y}}$:mean values for analyzed arrays.

Covariance (Equation 6) quantifies the variability of two factors relative to one another.

$$\boldsymbol{Covariance} = \frac{\sum(\boldsymbol{x} - \underline{\boldsymbol{x}})(\boldsymbol{y} - \underline{\boldsymbol{y}})}{\boldsymbol{n}}$$

Equation 6: Formula for covariance of a population, n: sample size.

These statistical indexes are used in the analysis of elements measured by XRF. The XRF unit used in this study provides a semi-quantitative spectrum of the concentrations of 40 different elements in the given sample. This study makes use of bulk rock XRF data collected by Core

Laboratories from mudstone cores from an undisclosed basin, and presents the results of statistical work for all elements in exception to those that were below the lower detection limit for the XRF unit and are likely not present in the sample (example Au and Ag). As XRF is a semi-quantitative tool it must be calibrated against a quantitative measure for reliable use. This study statistically compares elements measured by XRF to XRD calculated CEC for investigation of the elements stuck to clay mineral surfaces (exchangeable ions). These results are used to model CEC via linear regression and infer interactions between components of the rock. Exchangeable cations are sourced from rock components and are loose in the pore fluid if they are not stuck to a clay mineral surface A linear regression model is generated by a stepwise methodology where elements measured by XRF are ranked relative to calculated CEC. The elements are ranked based on correlation and covariance to measured or modeled CEC; higher correlations meaning higher rank. Elements with the highest rank are selected for regression modeling and then input into the Microsoft Excel LINEST function for the generation of regression constants. Elements are then added or removed based on their impact on the final correlation result; if the correlation values are improved, they are left in the equation. This process is repeated until the correlation between the modeled and the measured/calculated values no longer improves in the hundredths place. The result is a model for the extrapolation of CEC inferences across the dataset and a picture of the pore fluid composition from the statistical association. Measurement of CEC is addressed first, ideally these are used for the calibration of XRF CEC regression models.

Measuring CEC is a common practice in soil science and academic clay mineralogy studies; however, it is uncommon within most geotechnical applications. This is due to both the addition of sample surface area with grinding, and the time/expense associated with most lab-

based methods. By utilizing cobalt hexamine trichloride and inductively coupled mass spectrometry (ICP-MS) presents a cost-effective and rapid means of measuring CEC.

The samples must be diluted before measurement, and the exchangeable cations (Na, Ca, K, Mg) are bound to clay mineral surfaces with low concentration. Then the samples were diluted five times to bring the exchangeable ions within the measurable range of the ICP-MS unit. As a result, cobalt hexamine trichloride was still too large to reliably quantify. A 500 times dilution was required to make use of the cobalt hexamine trichloride data. If one wishes to measure both exchangeable cations and the concentration of the saturating solution within the same measurement run, they will need to prepare two of each sample. One set of samples with a 5 times dilution for measurement of exchangeable cations and another with a 500 times dilution for measurement of the saturating solution.

The ICP-MS unit measured the cobalt in solution, the results show a general linear increase with increasing sample grinding time (Figure 4, Figure 5, Figure 6, Figure 7). This is explained by an increase in particle surface area, which corresponds with more potential binding locations. The 100% montmorillonite sample appears to be an exception to this trend, instead of showing an increase in cobalt concentration (Figure 3). Measurement of exchangeable cations shows a general increase with increasing sample grinding times, this trend was particularly strong in the 100% illite, 100% kaolinite, and the mixed sample (Figure 9, Figure 10, Figure 12). The 100% montmorillonite sample did not show a significant change in exchangeable cation concentration with increasing grinding time. The montmorillonite results may be explained by the relative hardness of the mineral and the fact it was pre-powdered. In the pre-powdering process, the sample may have already been significantly broken down. CEC calculated from

measured exchangeable cations shows a general linear increase in values with increased sample grinding time (Figure 13).

Calculated CECs given in figure 13, are used to calculate a theoretical value for an unground sample following the Huff, (1987) method. Huff, (1987) found a strong association between the CEC calculated from measurement data from the shortest non-zero grind time measurement, Qv1, to that calculated from the next largest non-zero grind time measurement, Qvn, and the square root of grind time, in seconds (Huff, 1987). Huff, (1987) demonstrates the use of this association to extrapolate CEC values back to a theoretical unground state. He found this association to be applicable in clay poor sandstones and sandstones with up to 40% clay content. The applicability of this correction in mudstones is investigated by applying the correction to 100% clay samples. My results show a high correlation between Qvn/ Qv1 and the square root of sample grind time in mudstones (Figure 14, Figure 15, Figure 16, Figure 17, Figure 18). The correction reduces the initial non-zero grind time CEC by half or more, this value represents the amount of surface area the sample would likely have in-situ. The 100% montmorillonite and the 100% chlorite sample did not produce a strong correlation between Qvn/ Qv1 and the square root of sample grind time, these anomalous results may be due to sample hardness (Figure 14, Figure 18). In these cases, the first and last data points are used to generate a theoretical unground value, Qv0, with a stronger correlation. In both instances, these values do not vary greatly from the correlation generated from the weaker correlation.

Sample	Mineral Content (Weight %)	Pre-Grinding Sample Description
1	Montmorillonite (100%)	Fine Powder
2	Kaolinite (100%)	Fine Powder
3	Illite (100%)	Chips
4	Chlorite (100%)	Chips
5	Montmorillonite (24%) Kaolinite (25%) Illite (27%) Chlorite (24%)	Illite & montmorillonite chips in kaolinite and montmorillonite powder

Table 4: Samples used in grinding experiment.

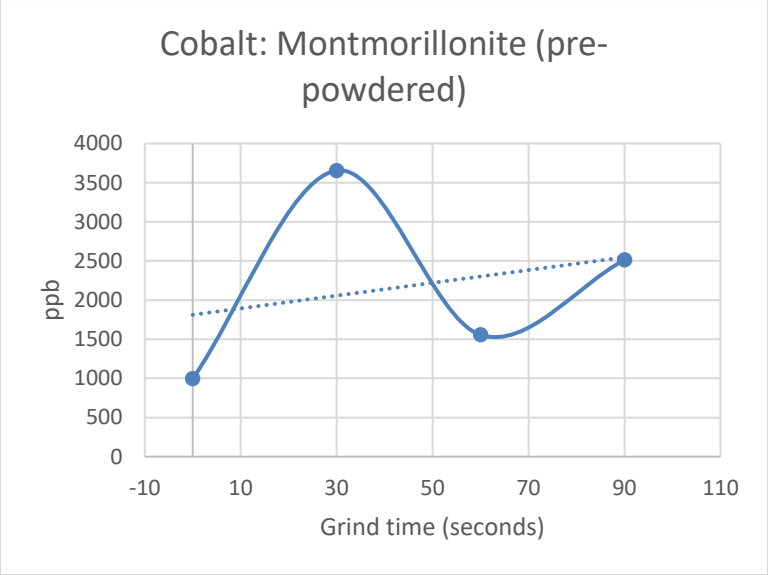

Figure 3: ICP-MS measured concentration of cobalt in solution, 100% montmorillonite sample.

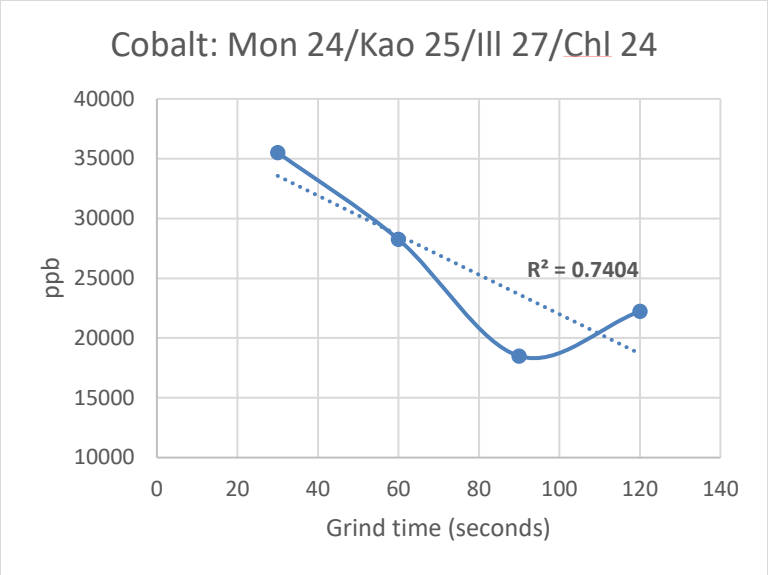

Figure 4: ICP-MS measured concentration of cobalt in solution, 24% montmorillonite, 25% kaolinite, 27% illite, 24% chlorite sample.

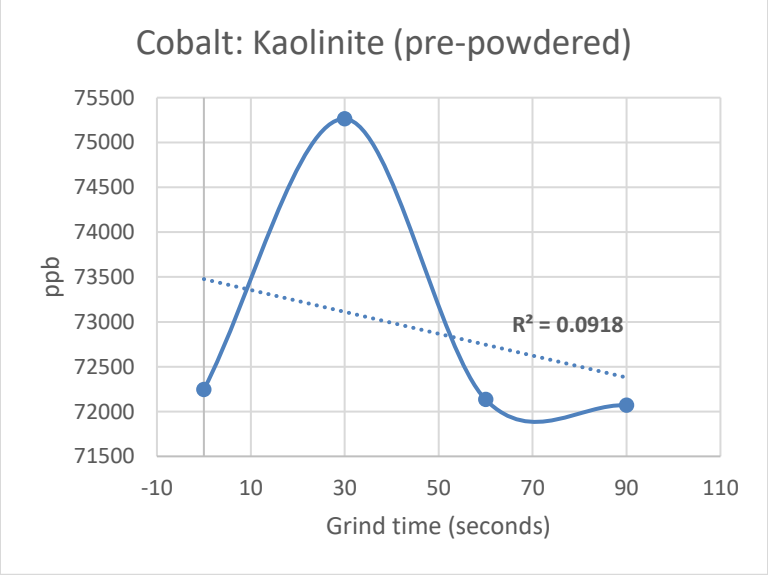

Figure 5: ICP-MS measured concentration of cobalt in solution, 100% kaolinite sample.

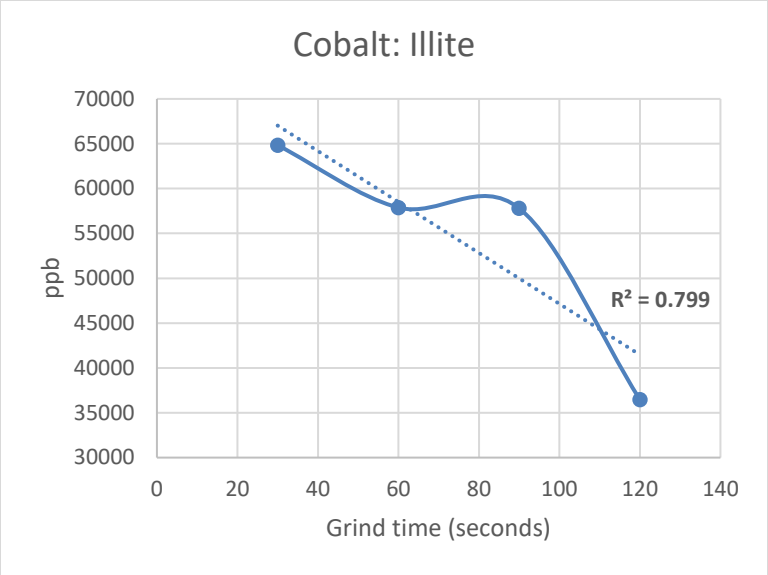

Figure 6: ICP-MS measured concentration of cobalt in solution, 100% illite sample.

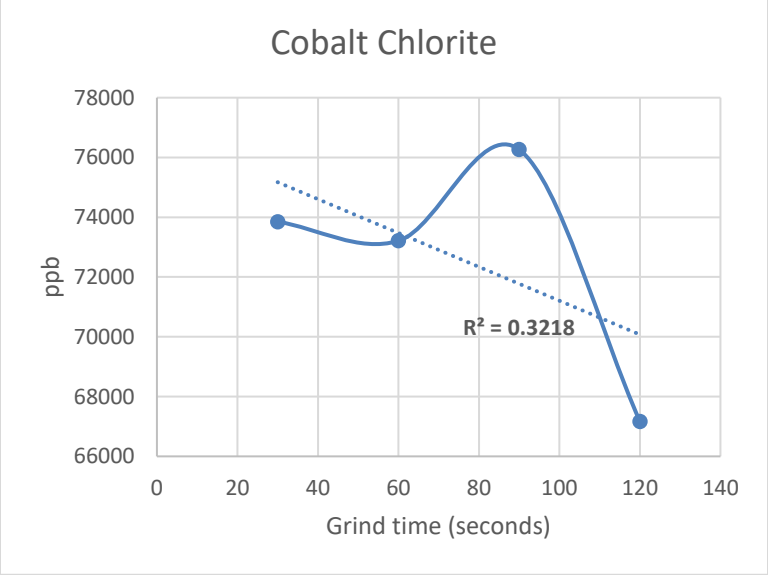

Figure 7: ICP-MS measured concentration of cobalt in solution, 100% chlorite sample.

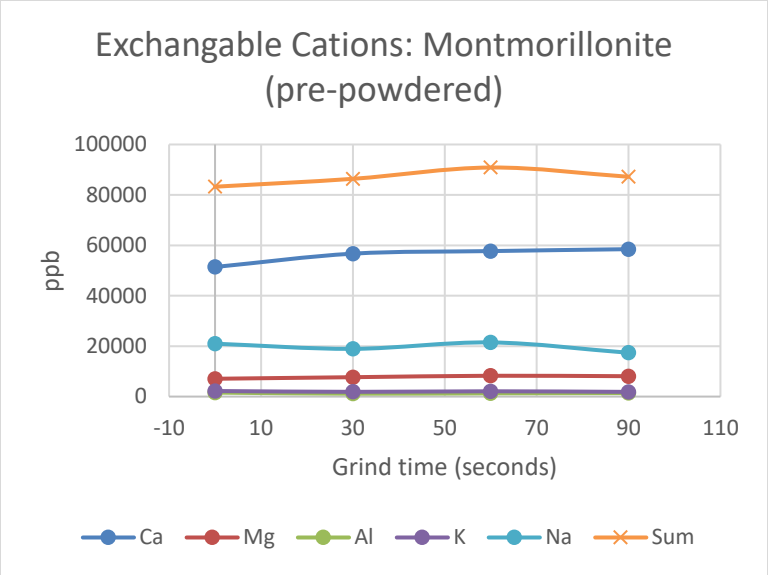

Figure 8: ICP-MS measured exchangeable cation results from solution, 100% montmorillonite sample.

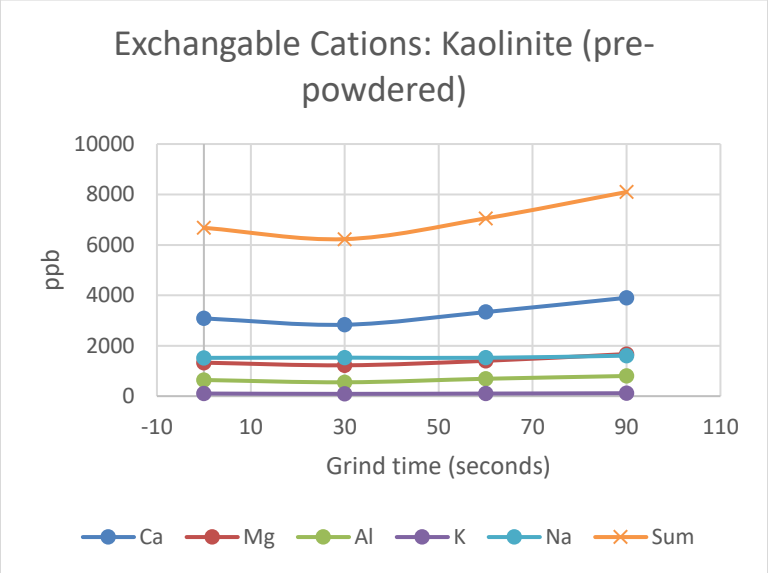

Figure 9: ICP-MS measured exchangeable cation results from solution, 100% kaolinite sample.

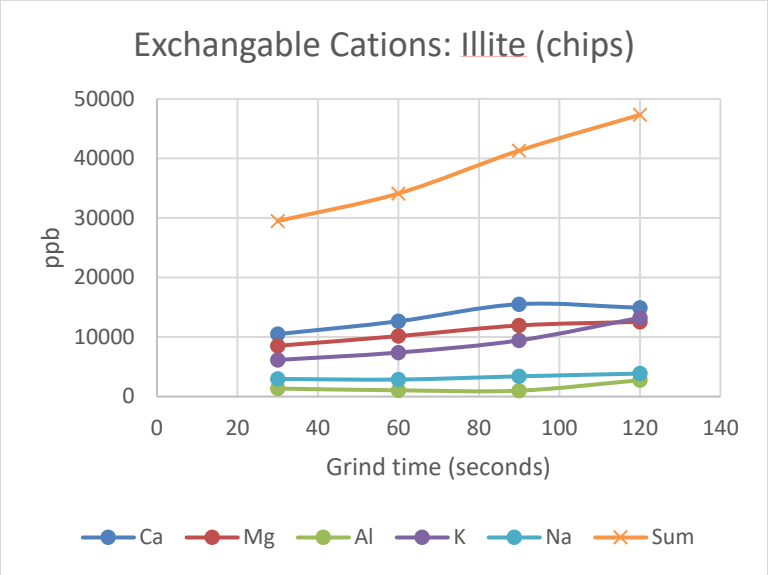

Figure 10: ICP-MS measured exchangeable cation results from solution, 100% illite samples.

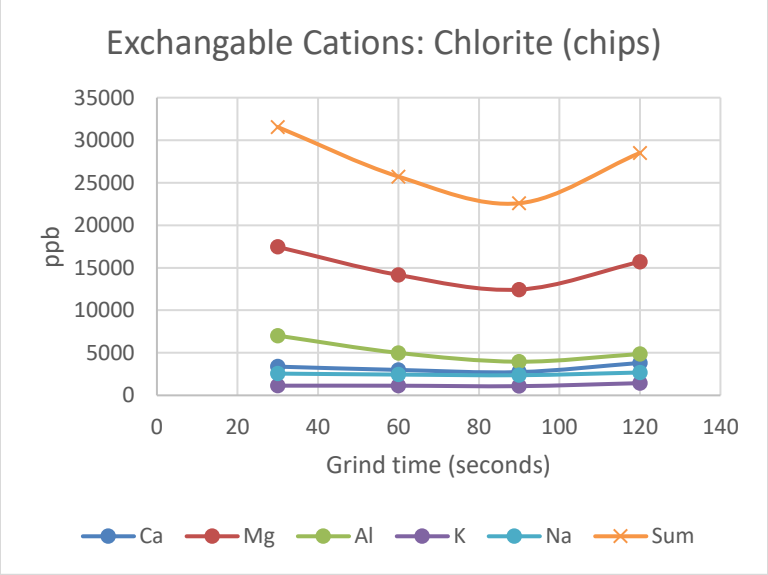

Figure 11: ICP-MS measured exchangeable cation results from solution, 100% chlorite sample.

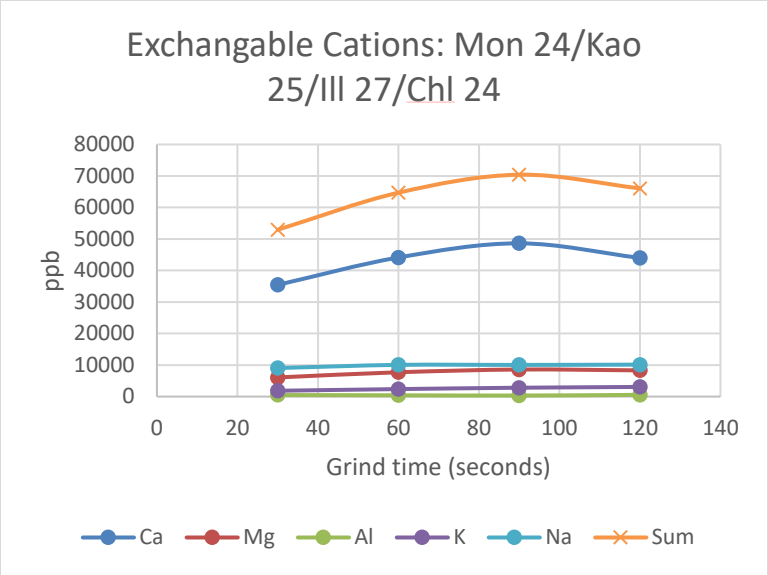

Figure 12: ICP-MS measured exchangeable cation results from solution, montmorillonite 24% kaolinite 25% illite 27% chlorite 24% sample.

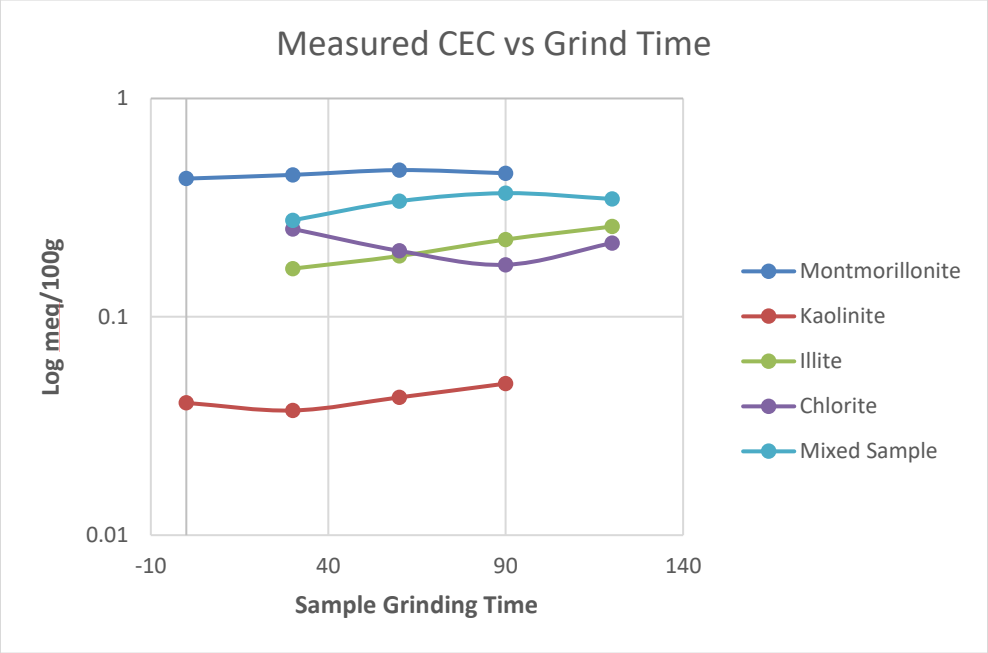

Figure 13: Log CEC calculated from measured exchangeable cations vs sample grinding time.

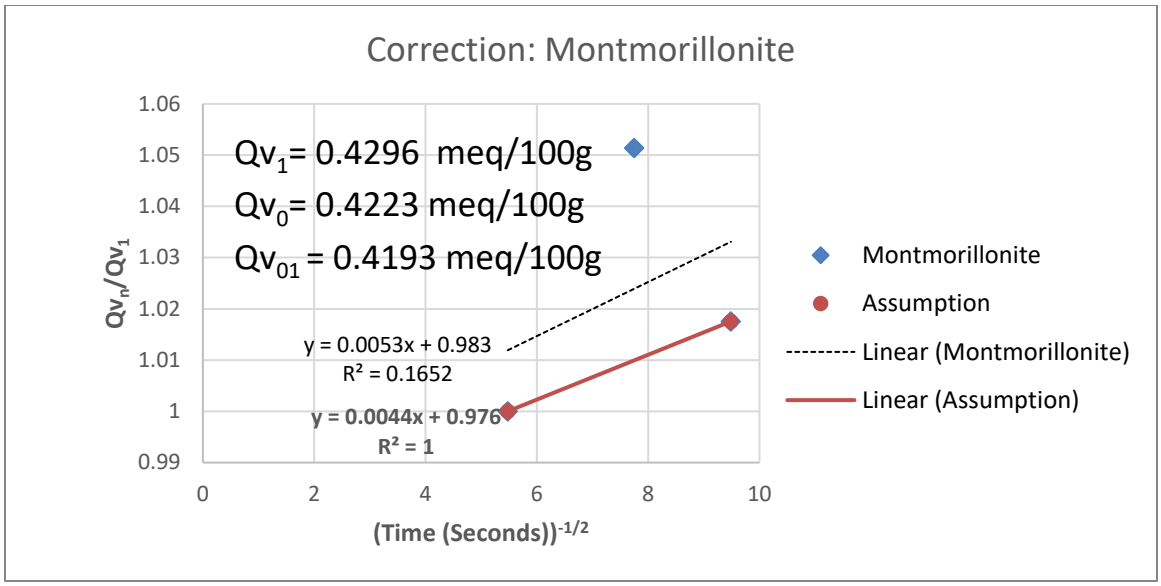

Figure 14: Correction plot for 100% montmorillonite sample. Ratio of shortest non-zero grind time CEC estimation (Qv_1) to subsequent grind time CEC estimation (Qv_n) vs the square root of grind time. Determined unground sample CEC (Qv_0) given on plot, Qv_{01} represents corrected value using only first and last data points.

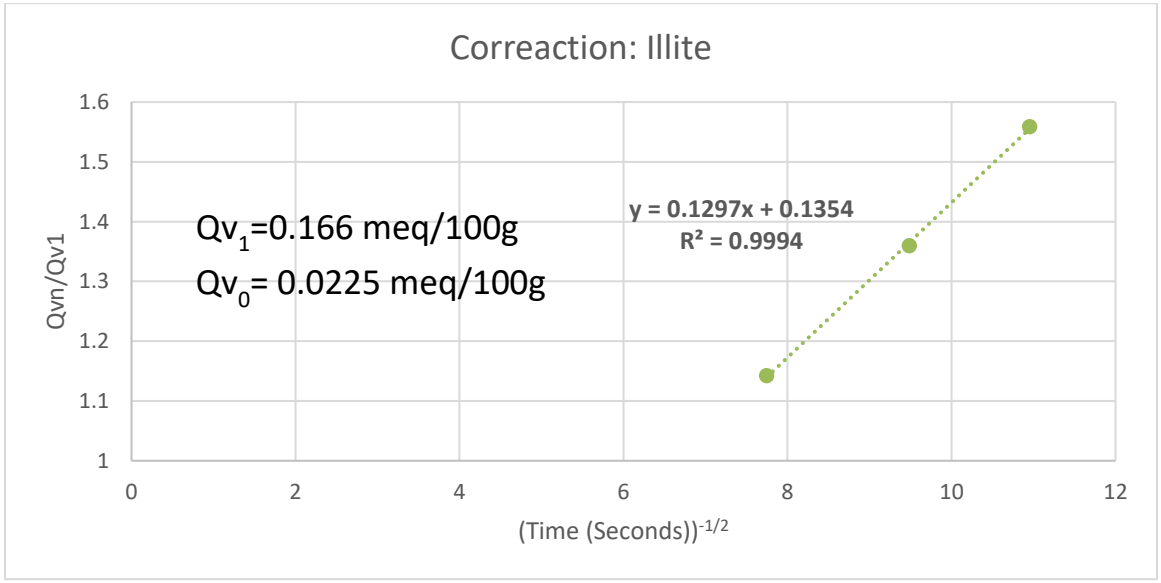

Figure 15: Correction plot for 100% illite sample. Ratio of shortest non-zero grind time CEC estimation (Qv_1) to subsequent grind time CEC estimation (Qv_n) vs the square root of grind time. Determined unground sample CEC (Qv_0) given on plot.

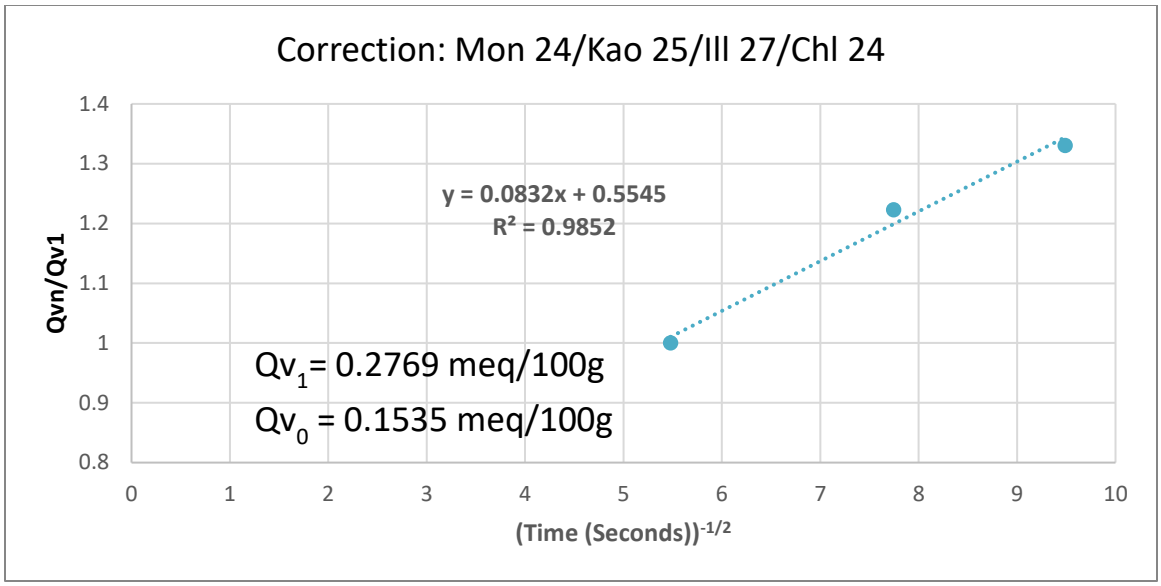

Figure 16: Correction plot for 24% montmorillonite, 25% kaolinite, 27% illite, 24% chlorite sample. Ratio of shortest non-zero grind time CEC estimation (Qv_1) to subsequent grind time CEC estimation (Qv_n) vs the square root of grind time. Determined unground sample CEC (Qv_0) given on plot.

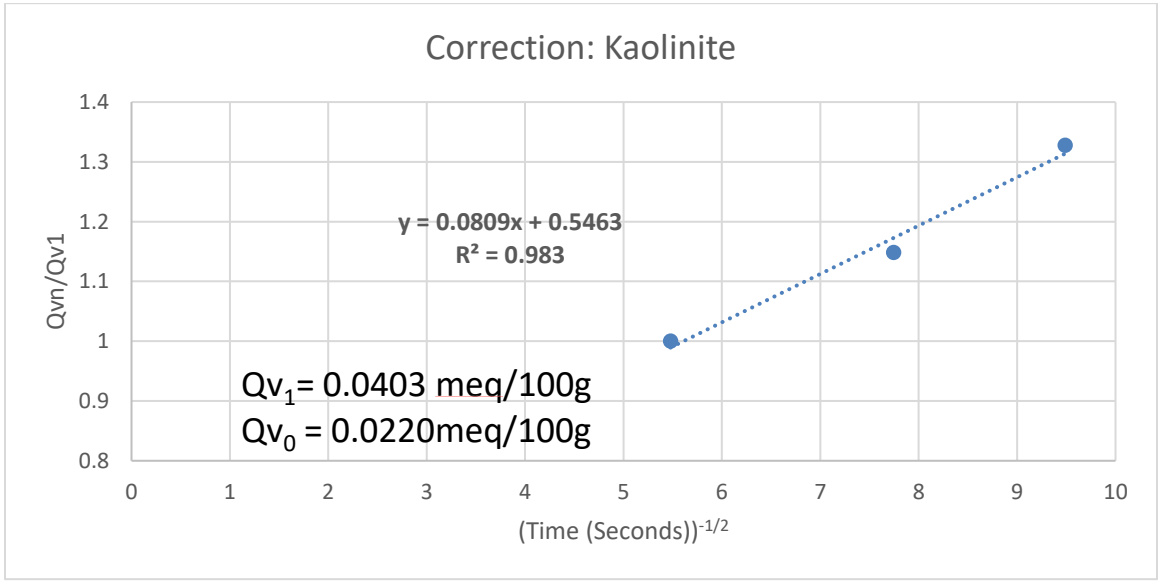

Figure 17: Correction plot for 100% kaolinite sample. Ratio of shortest non-zero grind time CEC estimation (Qv_1) to subsequent grind time CEC estimation (Qv_n) vs the square root of grind time. Determined unground sample CEC (Qv_0) given on plot, bolded value represents corrected value using only first and last data points.

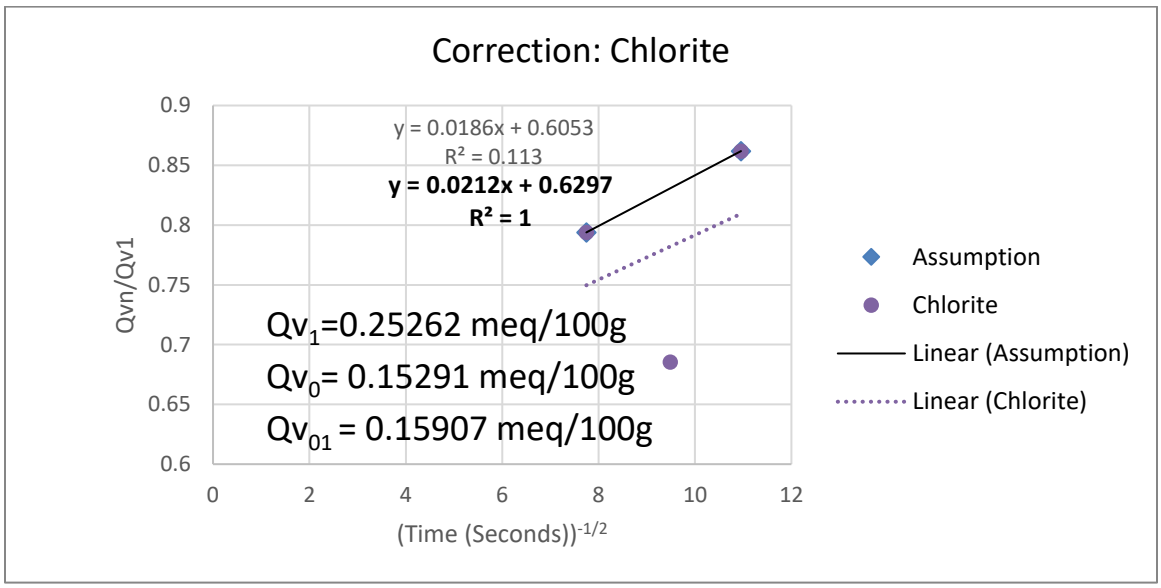

Figure 18: Correction plot for 100% chlorite sample. Ratio of shortest non-zero grind time CEC estimation (Qv_1) to subsequent grind time CEC estimation (Qv_n) vs the square root of grind time. Determined unground sample CEC (Qv_0) given on plot, Qv_{01} represents corrected value using only first and last data points.

Next, a linear regression model is generated for predicting CEC from XRF data in the interest of high-resolution formation evaluation in core-based studies. Sharma et al. (2015) is referenced for method and initial regression variables. First, XRF data is normalized to remove effects of scale and then analyzed for correlation (Equation, 9) and covariance (Equation, 10) vs XRD calculated CEC (Equation 4, Figure 1, Figure 2). The resulting correlation and covariance values are used to rank each element, for the selection of regression variables.

The elements with the highest correlation and covariance values were selected and input into Microsoft Excel's LINEST function (least-squares multivariable linear regression function) for the determination of constants. An R^2 value is then calculated from the LINEST generated

model and the XRD calculated CEC. Variables in the regression with the lowest correlation and covariance are then swapped to improve the R^2 value, this process continues until the R^2 values stabilize at the maximum possible value for the given data inputs. My modeling of CEC selected the elements As, Ni, Fe, Ti, P, Cl, S, and XRD $Clay$ ($wt\%$) as the optimum variables for prediction of CEC across the entirety of my dataset, assuming XRD calculated CEC is an accurate representation of clay properties, , the final R^2 being 0.9256 (Figure 19). The formula has a decent correlation with calculated CEC in all rocks in the basin and was found to have an improved correlation if calibrated for an individual well or geologic unit within a well.

The selected variables provide insight into the interaction between the components comprising the rock. First, we are provided information regarding elements potentially incorporated in the study's clay mineral structures (Fe and Ti), pore fluid (P, Cl, and S), and those with organic matter (As and Ni). This is assuming pore fluid and redox elements are sticking on the surface of the clay minerals. Ions possibly associated with pore fluid are also common components in salts, this may explain salt formation on recovered cores in storage. XRD clay weight percent provides stabilization for the function, suggesting that clays are the primary contributor to CEC; this may be influenced by the utilization of CEC calculated from XRD. However, Sharma et al. (2015) utilized measured CEC values from soils in their calculations also found that R^2 values were improved by the inclusion of weight percent clay. Greater values may be generated when the analysis is completed over a single well, formation, or unit. This provides means for generating high-resolution CEC curves for detailed analysis of fluid movement within a formation. XRF is relatively inexpensive to collect and is a powerful tool for characterizing petroleum reservoir clay properties when calibrated with calculated XRD or wet chemistry measured CEC values.

These improvements increase the utility of measured CEC in geoscience and provide improved means of understanding the processes by which rocks dewater.

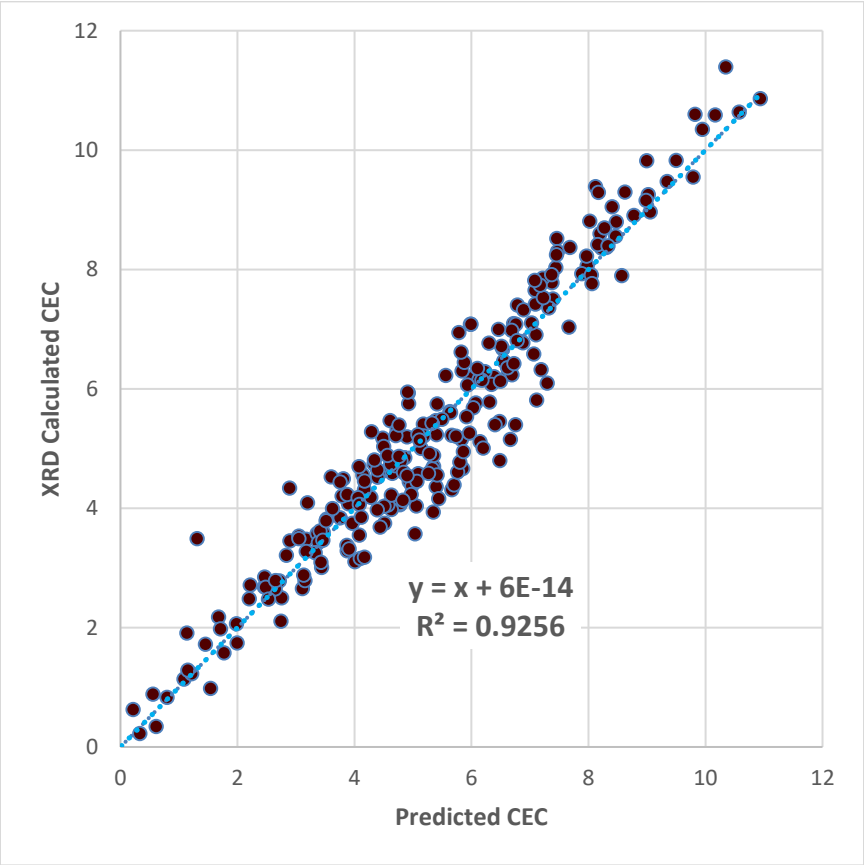

Figure 19: XRF modeled CEC estimations vs XRD calculated CEC values.

This study compares DI to crushed shale measured porosity, grain density, water saturation, XRD measured mineralogy, hydrogen and oxygen index measured from pyrolysis organic data. This data is sourced from a Core Laboratories database of standard core analyses they collected from an undisclosed basin.

The range of DI values for the basin are 0.15 and 12.37. XRD measured weight percent values for individual clay species are compared to DI, but does not show a strong trend (Figure 20, Figure 21, Figure 22, Figure 23, Figure 24). Discrete smectite is not plotted due to a lack of data. The exception to this is the smectite fraction in mixed-layer illite-smectite, which decreases with increasing DI (Figure 24). This is likely due to the conversion of smectite to illite, during this conversion the rock loses binding potential, bulk mixed layer illite-smectite suggests a similar association (Figure 21) (Pollastro, 1990),

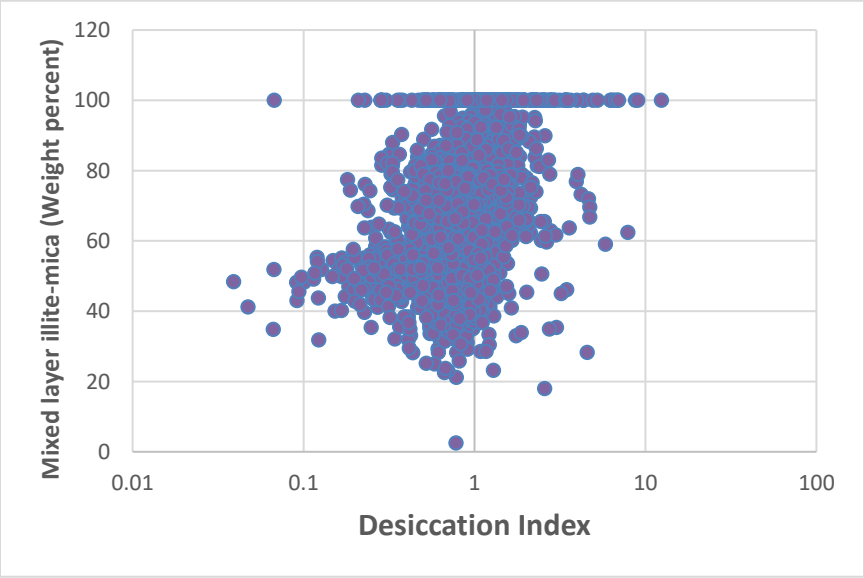

Figure 20: XRD powder diffraction measured mixed layer illite-mica vs log desiccation index to emphasize trend.

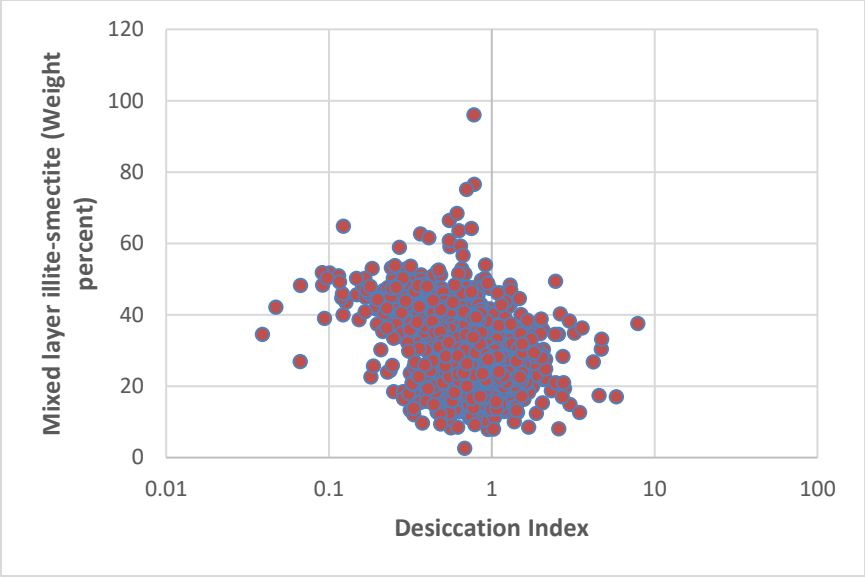

Figure 21: XRD powder diffraction measured mixed layer illite-smectite vs log desiccation index to emphasize trend.

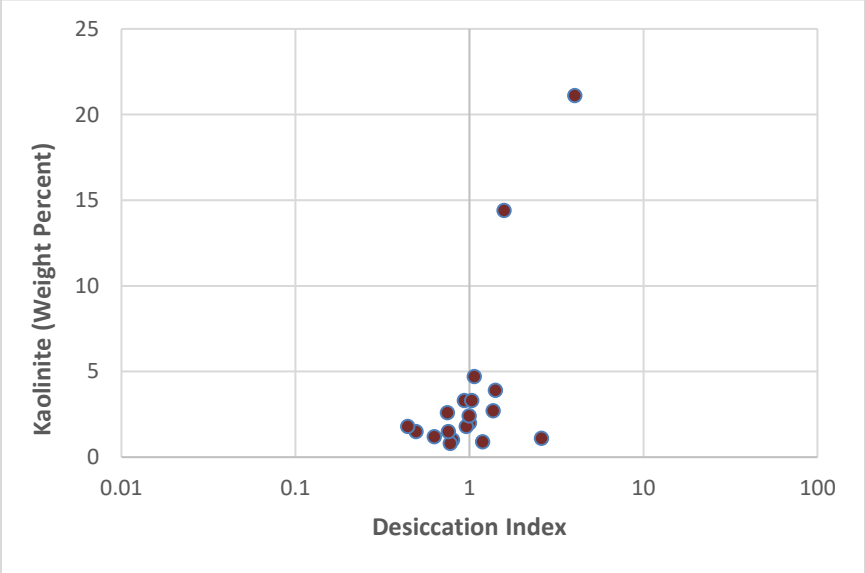

Figure 22: XRD powder diffraction measured kaolinite vs log desiccation index to emphasize lack of trend.

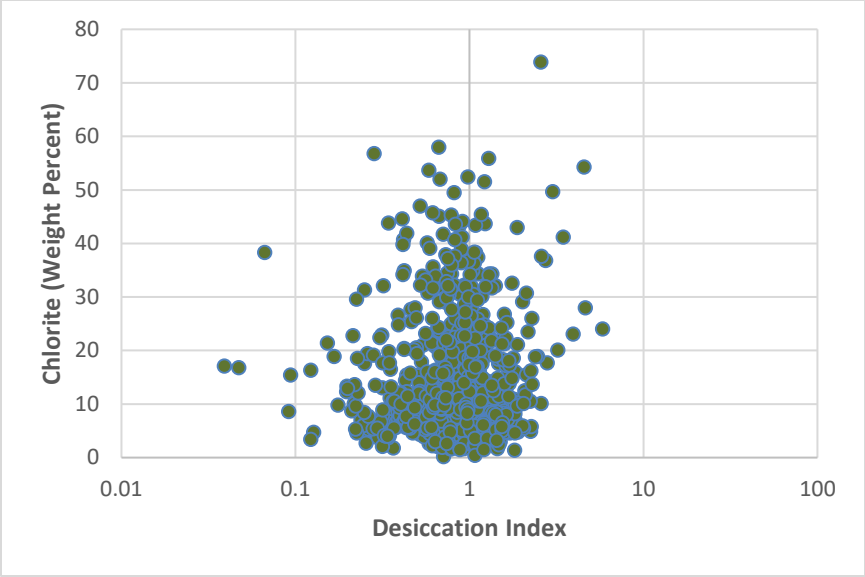

Figure 23: XRD powder diffraction measured chlorite vs log desiccation index to emphasize lack of trend.

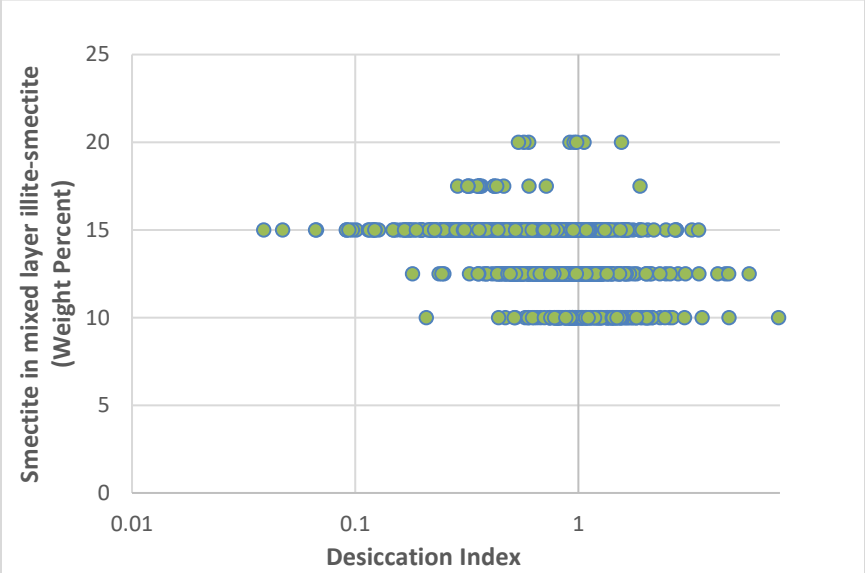

Figure 24: XRD powder diffraction measured smectite in mixed layer illite-smectite vs desiccation index log desiccation index to emphasize trend.

The comparison of all basin grain density values to DI does not show a trend, suggesting that their association is indirect (Figure 25). Comparison of desiccation to total porosity and water saturation show positive correlation, increased values in DI are associated with greater water and porosity values (Figure 26, Figure 27). Inversely, higher values for total clay content are associated with lower DI values (Figure 28).

Figure 25: Crushed shale analysis grain density vs desiccation index.

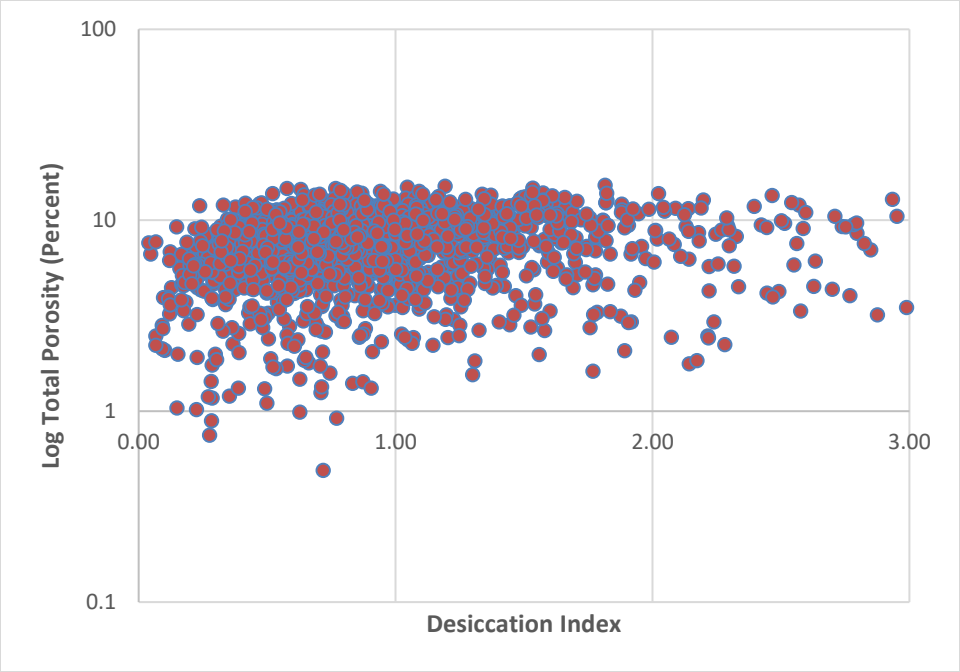

Figure 26: Crushed shale analysis total porosity vs log desiccation index to emphasize trend.

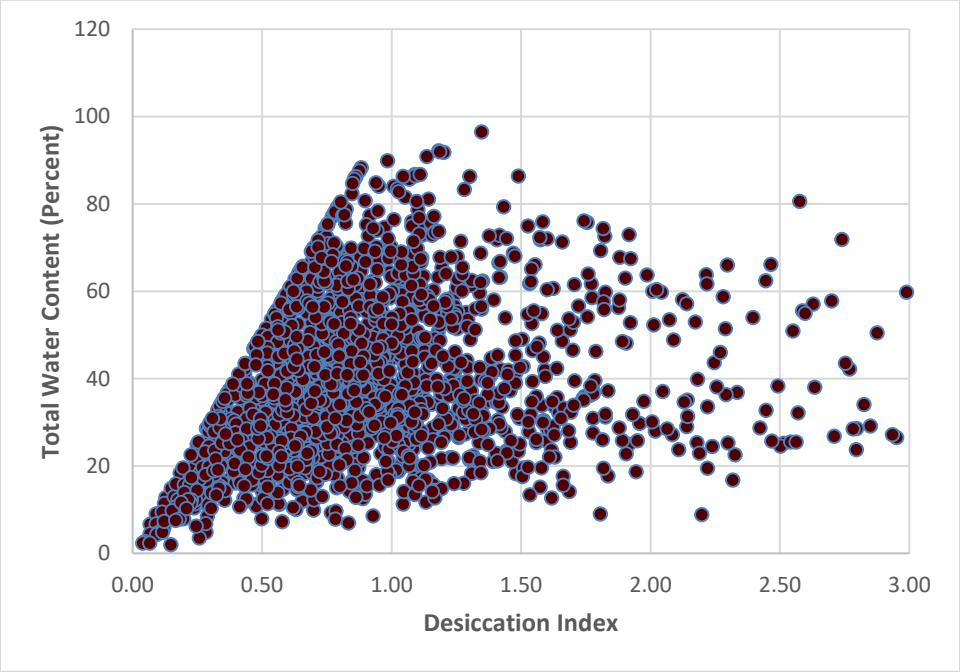

Figure 27: Crushed shale analysis total water content vs desiccation index. Equation of lower DI value bounding line Y= X*0.84/83.27.

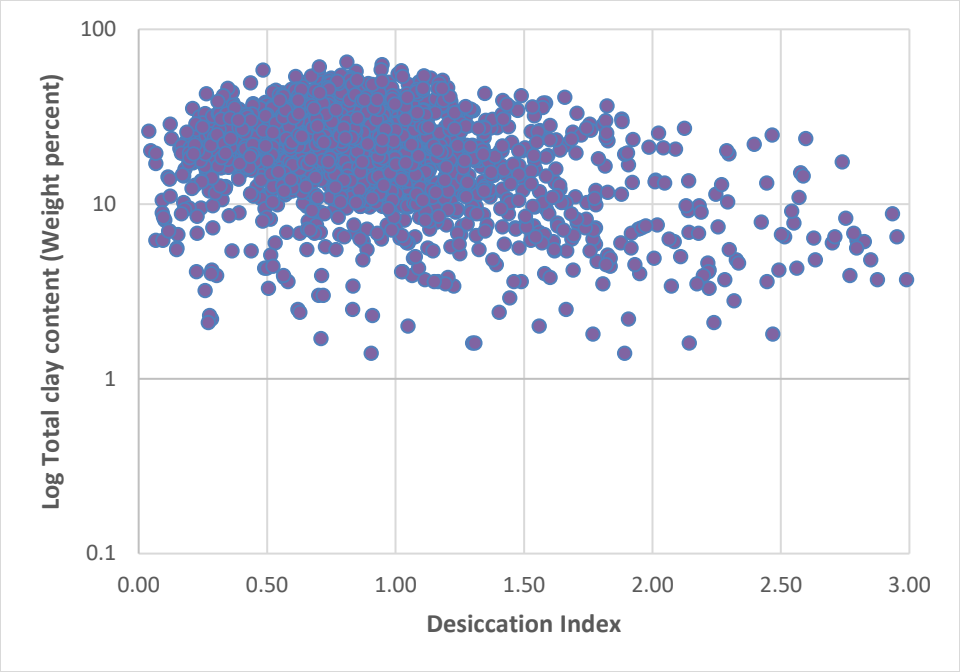

Figure 28: XRD powder diffraction total clay content vs log desiccation index to emphasize trend.

The correlation of low porosity and water saturation values with DI suggests that desiccation is a function of storage. Total water saturation refers to all the water within the rock. This volume of fluid must be accommodated somewhere within the available pore space. It is easier for a rock to desiccate if the volume of water to be displaced is small. Clay content provides a component of water that is chemically bound. This mineral bound water fills the pore space and is difficult to displace, which is where the term “effective porosity” originates. Grain density is the weight of all solid components in a sample divided by the total volume. Measured grain density has high scatter as it does not distinguish between clays and framework grains which could strongly skew results. However, in modeling where all other factors are controlled, larger grain density is associated with lower DI values.

The organic material in this dataset is mature and predominantly type 1 and type 2 kerogen (Figure 31). High hydrogen index values associated with relatively low oxygen index values (Tissot and Welte, 1984). The high grade of organic thermal maturity is congruent with the high degree of inorganic thermal maturity suggested by the clustering of smectite in mixed layer illite-smectite between ten and twenty percent. Mixed layer smectite will stabilize at about ten percent in high thermal maturity cases (Pollastro, 1990). There is a negative correlation between total organic content and DI (Figure 29). Also, there is a negative association between the ratio of hydrogen index and oxygen index, and DI (Figure 30). This suggests that rocks with greater concentrations of organic content and richness may be more effective at displacing water. However, rocks with lower degrees of organic richness may not have been able to produce volumes of hydrocarbons enough to displace water.

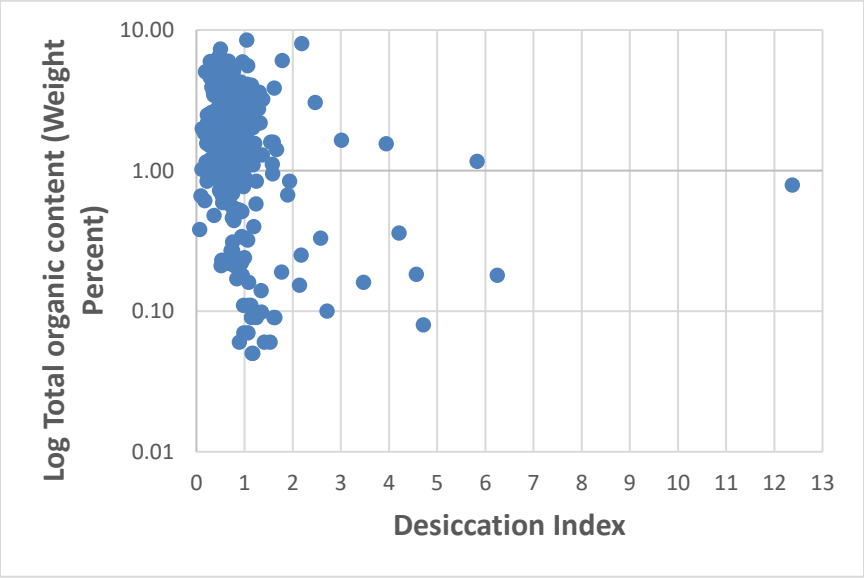

Figure 29: Pyrolysis total organic content vs desiccation index.

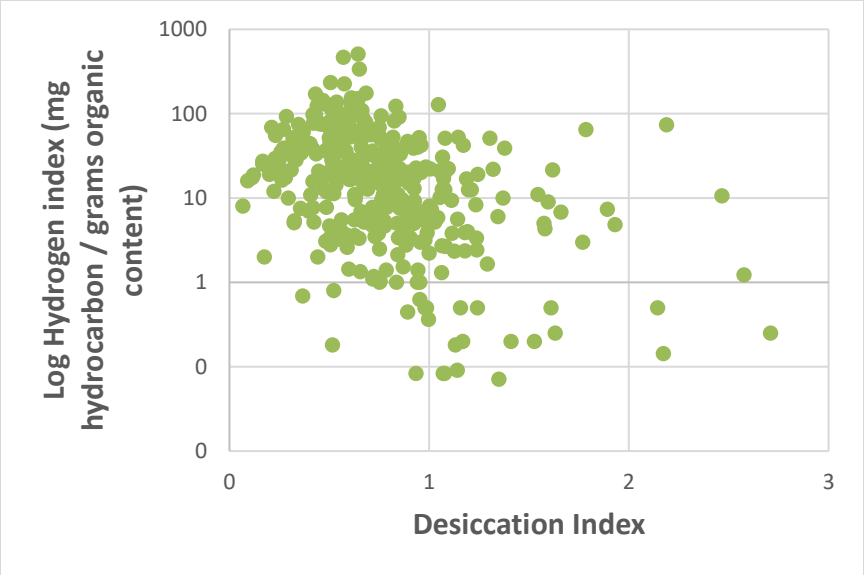

Figure 30: Ratio of pyrolysis hydrogen index to pyrolysis oxygen index vs desiccation index.

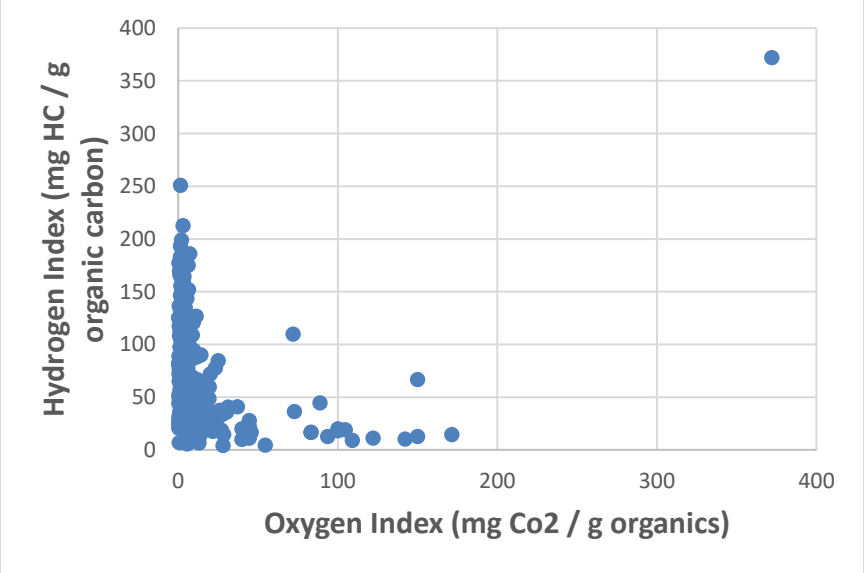

Figure 31: Van Krevelen type diagram, pyrolysis hydrogen index vs pyrolysis oxygen index.

The association of clay with desiccation is also evidenced in elements measured by XRF. Elements commonly associated with clay mineral structures (namely Ca, K, Al, Si, S, and Mg) show high association with DI, clay bound water, and bulk volume water (Figure 35, Figure 36, Figure 37). XRF data also shows a strong association of redox elements with DI, clay bound water, and bulk volume water (Figure 32, Figure 33, Figure 34).

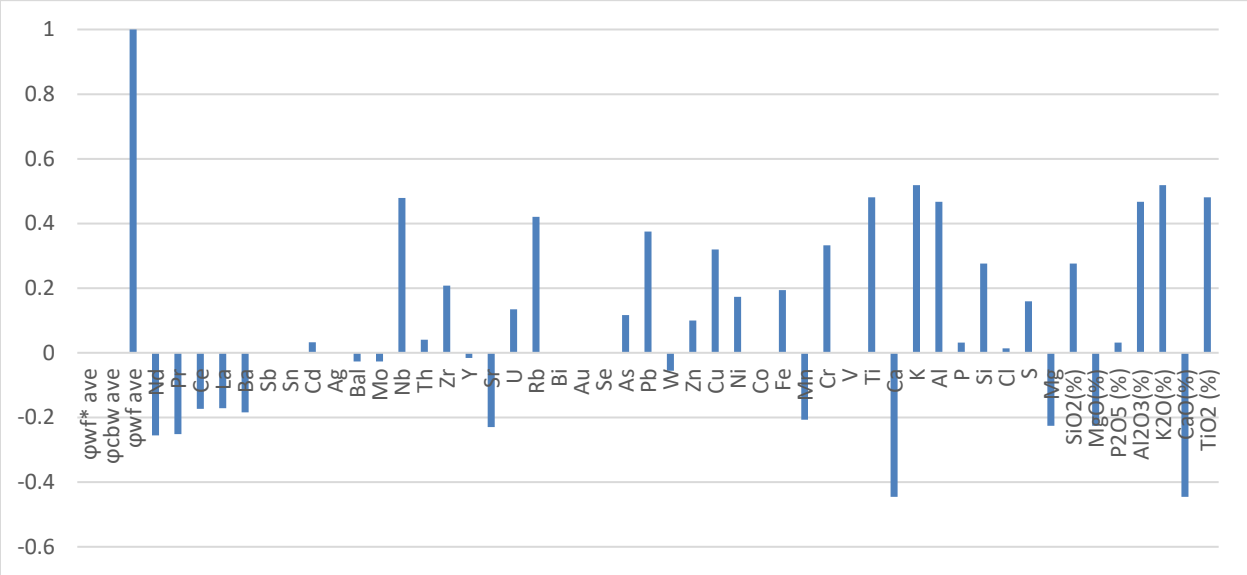

Figure 32: Elements measured by XRF correlation with bulk volume water results. Bars represent correlation of bulk volume water to the element listed below bar.

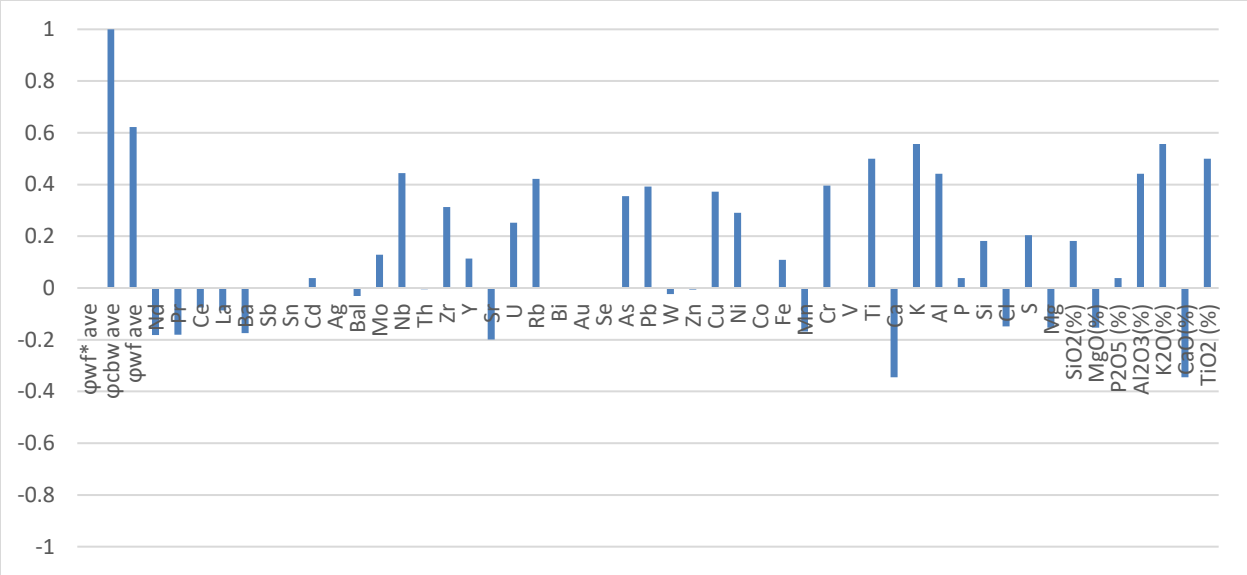

Figure 33: Elements measured by XRF correlation with clay bound water results. Bars represent correlation of clay bound water to the element listed below bar.

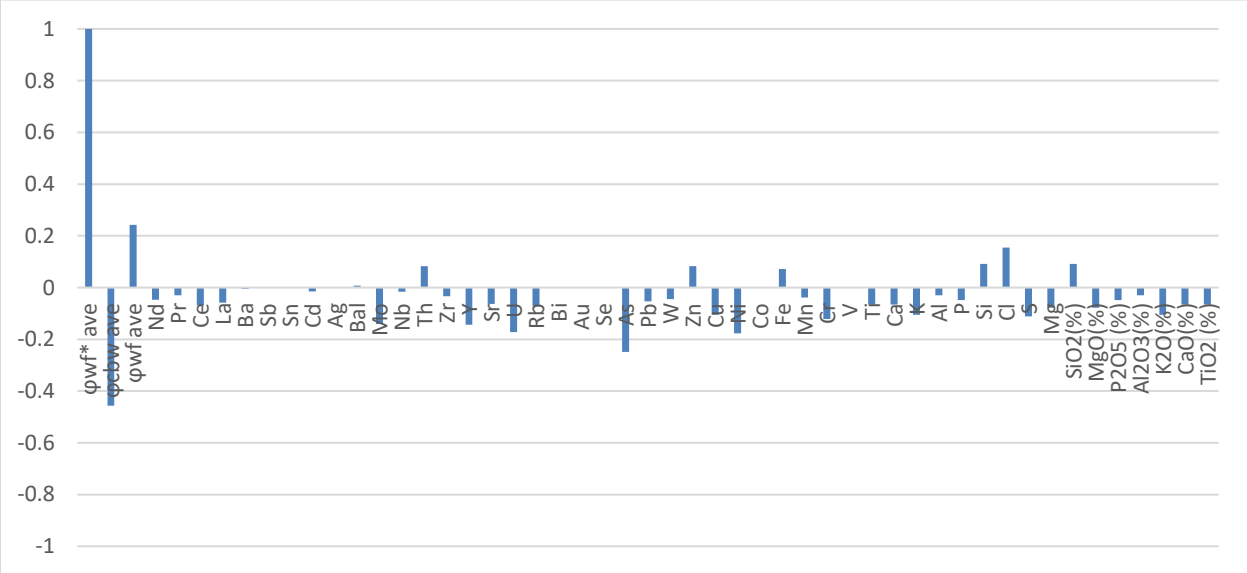

Figure 34: Elements measured by XRF correlation with desiccation index results. Bars represent correlation of desiccation index to the element listed below bar.

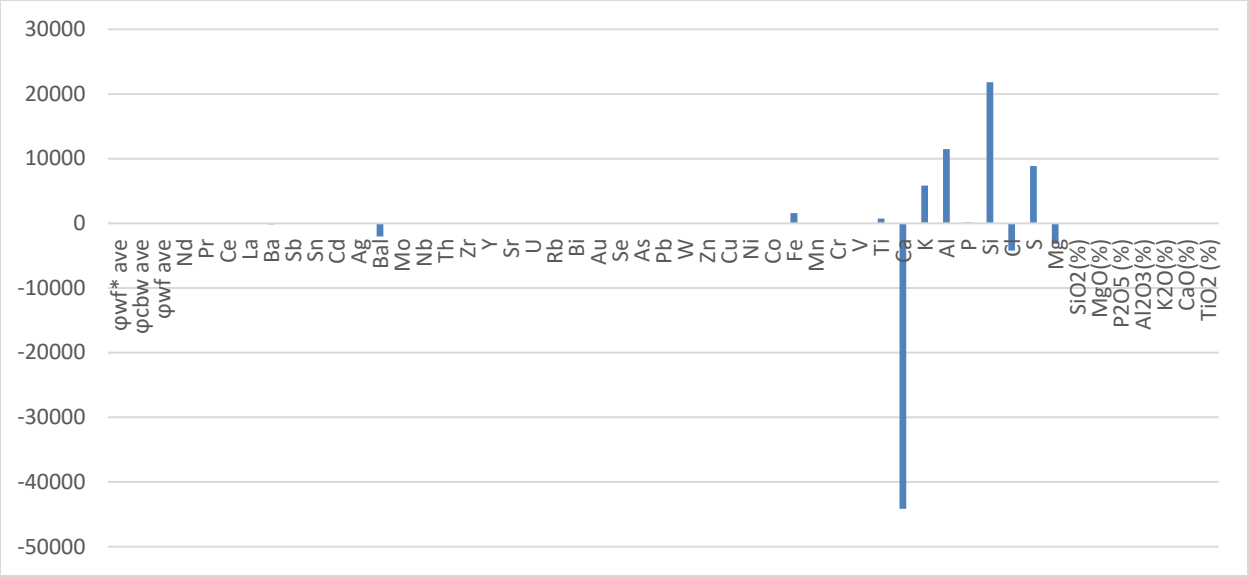

Figure 35:Elements measured by XRF covariance with clay bound water results. Bars represent covariance of clay bound water to the element listed below bar.

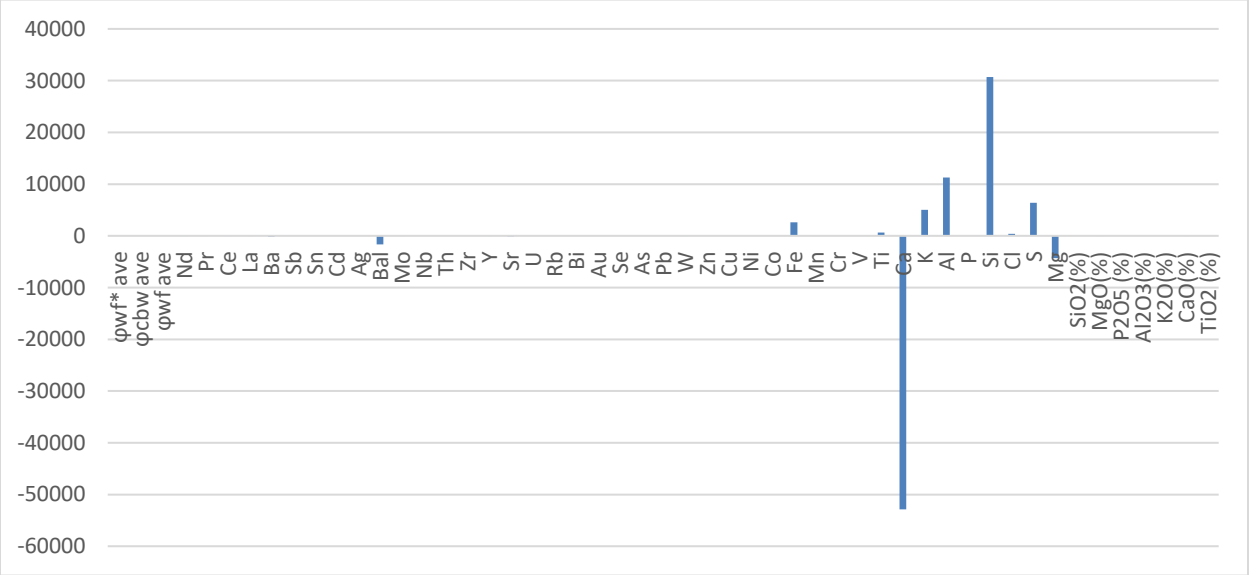

Figure 36: Elements measured by XRF covariance with bulk volume water results. Bars represent covariance of bulk volume water to the element listed below bar.

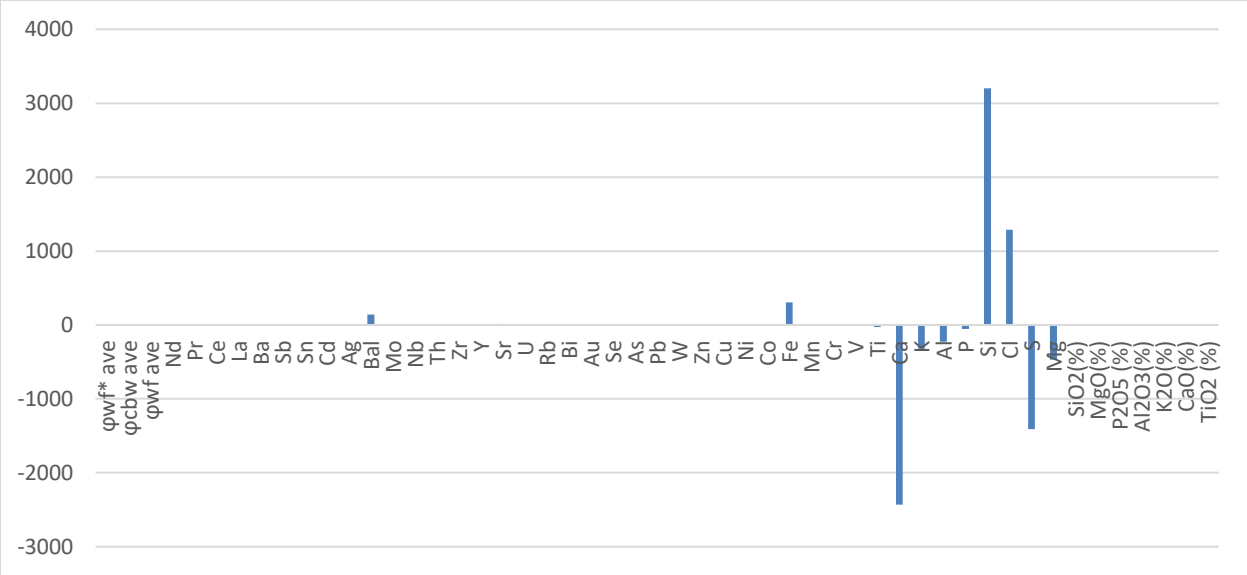

Figure 37: Elements measured by XRF covariance with desiccation index results. Bars represent covariance of desiccation index to the element listed below bar.

The potential degree of desiccation in a rock is controlled by the volume or mass of clay, CEC of the clay present, and total porosity. The total clay present and distribution of clay mineralogy controls the sub-irreducible water capacity of the rock. Hypothetically, chlorite may be the greater contributor to whole rock CEC than smectite due to the relative abundance of present clay minerals. Thusly, consideration of the rock's modal mineralogy may improve the selection of injected production enhancing compounds (i.e. clay inhibitors). Porosity influence's the volume of water necessary to displace with hydrocarbon production for desiccation. This generation controls the volume of water displaced and is controlled by organic type and maturity. Consequently, much of a rock's potential for desiccation is determined by lithology. When comparing bulk volume water to water potentially bound to clays, trends in the data become apparent when data points are sorted based on depositional processes (Figure 38, Figure 39,

Figure 40, Figure 41, Figure 42). Depositional processes control the availability of rock-forming materials and the processes they may undergo post-deposition. For example, a restricted basin will generally provide a lower energy environment for deposition, skewing particle sizes into the clay to silt size. This decreases the total porosity in the rock and increases the abundance of clay, resulting in a stronger CBW fraction and likely a lower corresponding DI value.

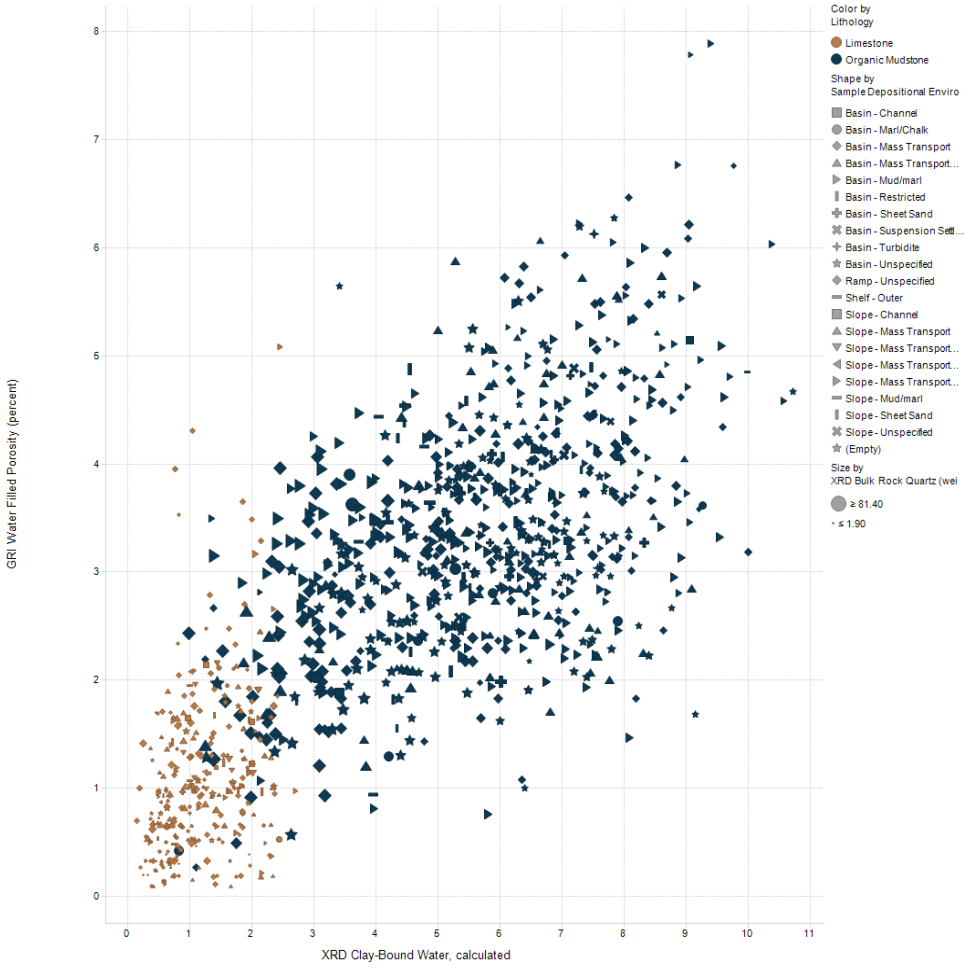

Figure 38: DI scatterplot, x-axis: calculated clay-bound water, y-axis: water filled porosity (bulk volume water), points sized by weight percent quartz as determined by XRD, symbols indicate sample depositional environment, colors indicate sample lithology as described in legend.

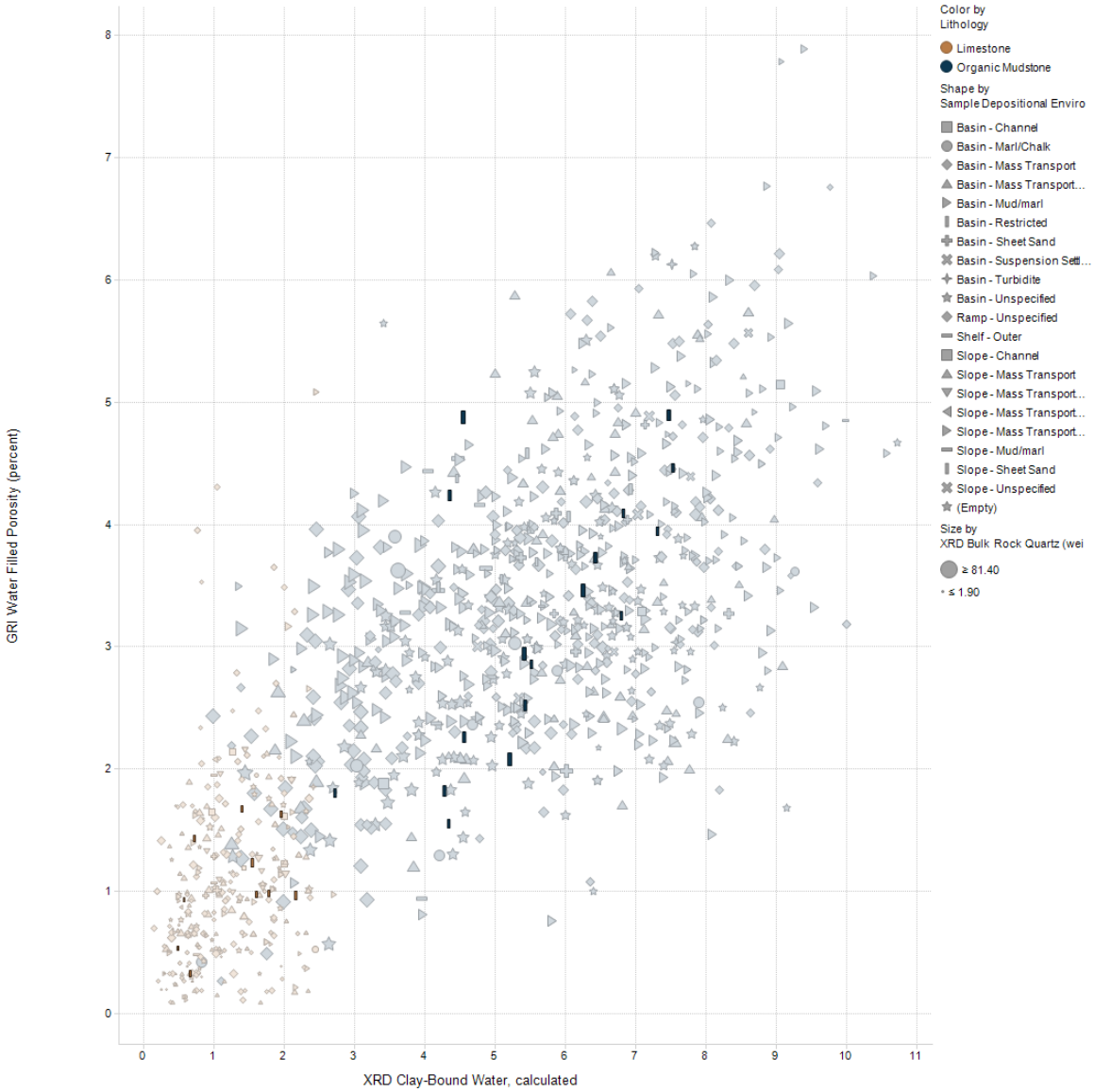

Figure 39: DI scatterplot, x-axis: calculated clay-bound water, y-axis: water filled porosity (bulk volume water), points sized by weight percent quartz as determined by XRD, symbols indicate sample depositional environment, colors indicate sample lithology as described in legend. Figure emphasizes slope sheet sands.

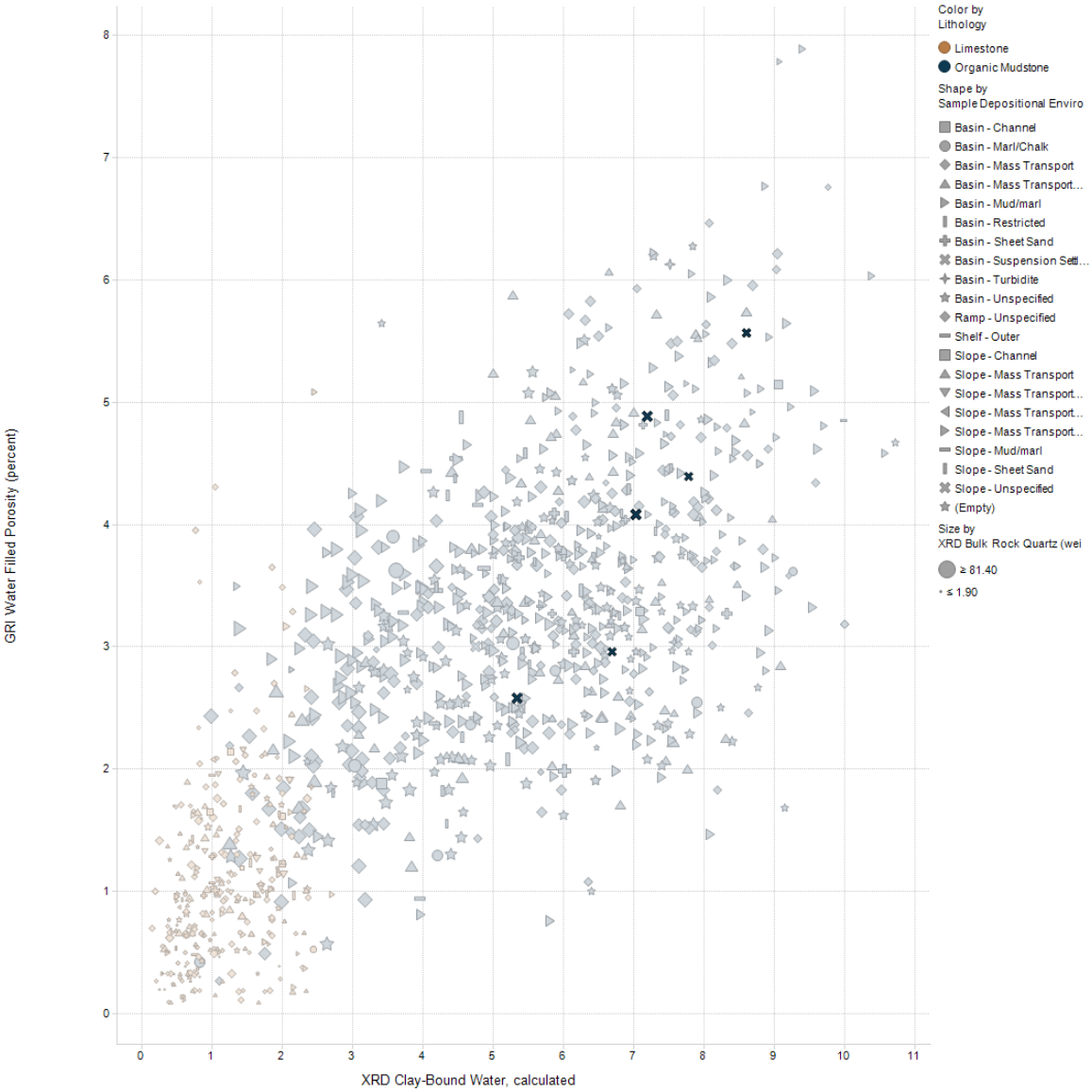

Figure 40: DI scatterplot, x-axis: calculated clay-bound water, y-axis: water filled porosity (bulk volume water), points sized by weight percent quartz as determined by XRD, symbols indicate sample depositional environment, colors indicate sample lithology as described in legend. Figure emphasizes basin suspension.

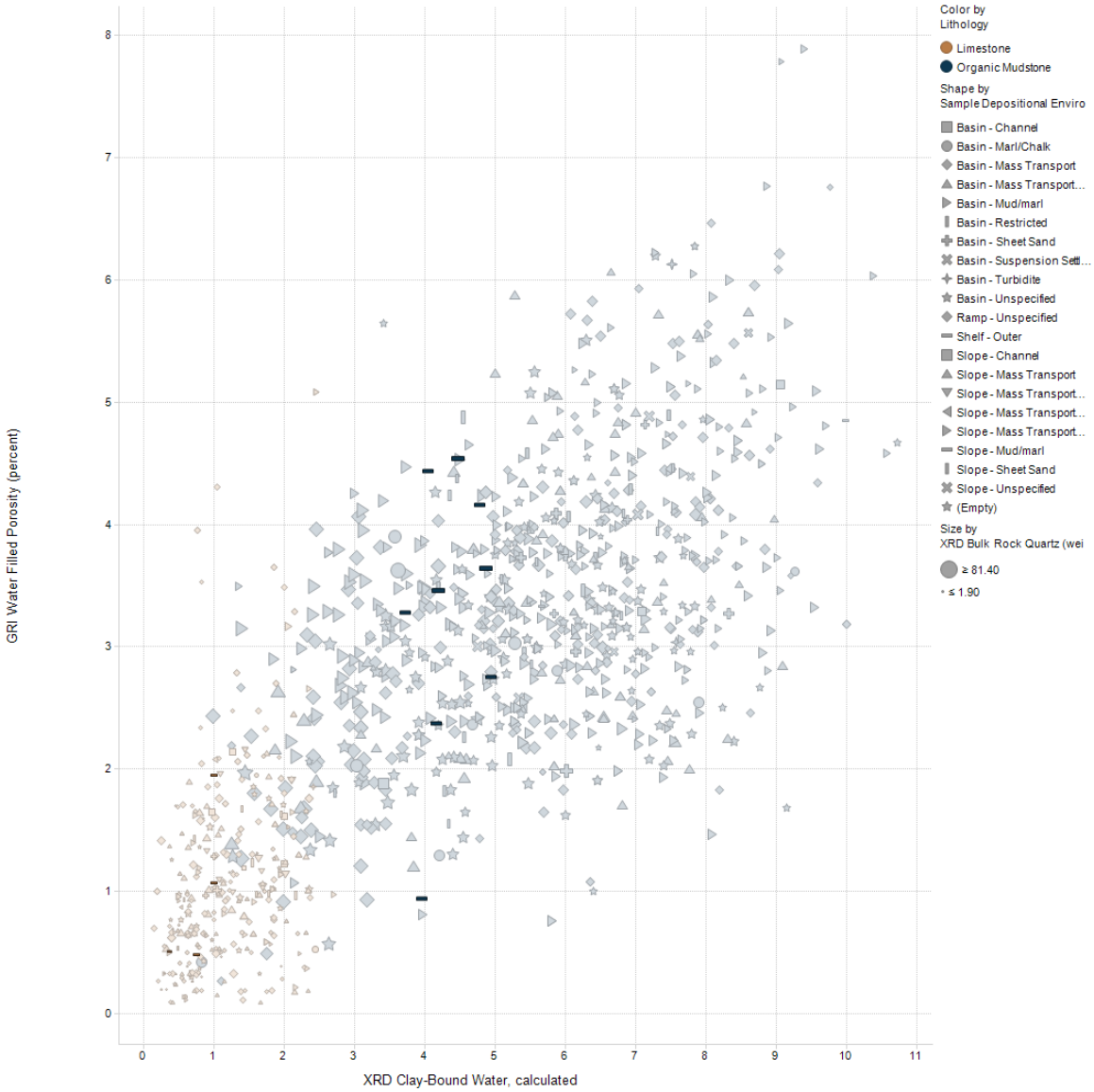

Figure 41: DI scatterplot, x-axis: calculated clay-bound water, y-axis: water filled porosity (bulk volume water), points sized by weight percent quartz as determined by XRD, symbols indicate sample depositional environment, colors indicate sample lithology as described in legend. Figure emphasizes slope mud/marls.

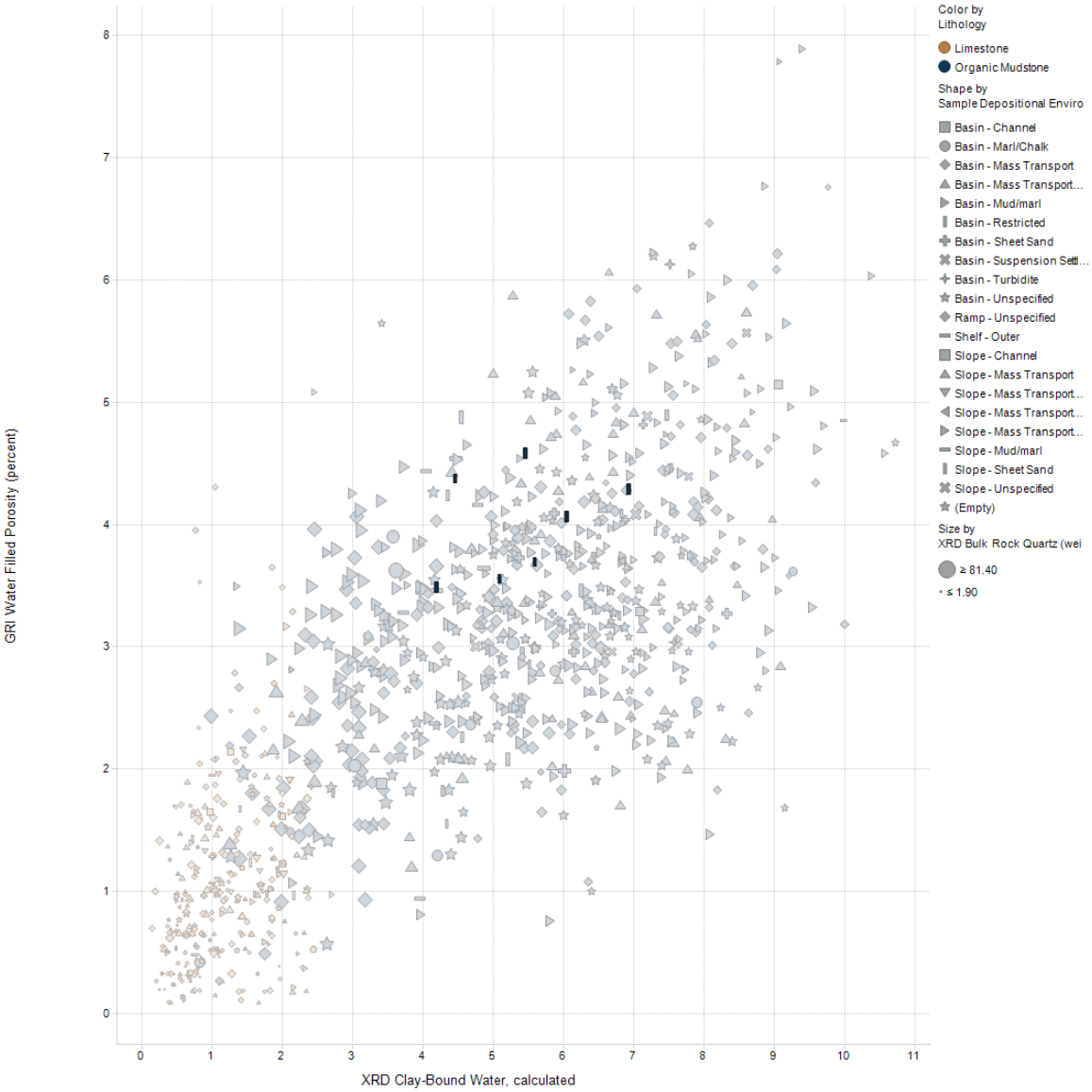

Figure 42: DI scatterplot, x-axis: calculated clay-bound water, y-axis: water filled porosity (bulk volume water), points sized by weight percent quartz as determined by XRD, symbols indicate sample depositional environment, colors indicate sample lithology as described in legend. Figure emphasizes restricted basin depositional environment.

Monte Carlo simulations are run to observe the interaction between the variables and equations involved in the calculation of reservoir desiccation. The purpose of this simulation is to mathematically investigate the relative influence on varying rock properties on final

desiccation values. This provides important knowledge of the relative influence of varying rock properties on desiccation and the degree of change potentially expected. To begin, all involved variables are set to a constant value listed in table 5, and then individually varied to investigate their relative influence on DI.

Variable	Control Values
Grain Density (g/cc)	2/656 (Dataset Average)
Total Porosity (Volume %)	8 (Dataset Average)
Water Saturation (Volume %)	40.41 (Dataset Average)
Salinity (g/L)	30.5870 and 166.287 (High as low estimations
Total Clay (Weight %)	15
Mixed layer illite/smectite (Weight %)	12
Illite in mixed layer illite/smectite (Weight %)	20
Illite/Mica (Weight %)	40
Mixed layer chlorite/smectite (Weight %)	8
Chlorite in mixed layer chlorite/smectite (Weight %)	30
Smectite (Weight %)	5
Kaolinite (Weight %)	20
Chlorite (Weight %)	15

Table 5: Input variables for Monti Carlo simulation. The calculated desiccation value from these inputs is 1.255.

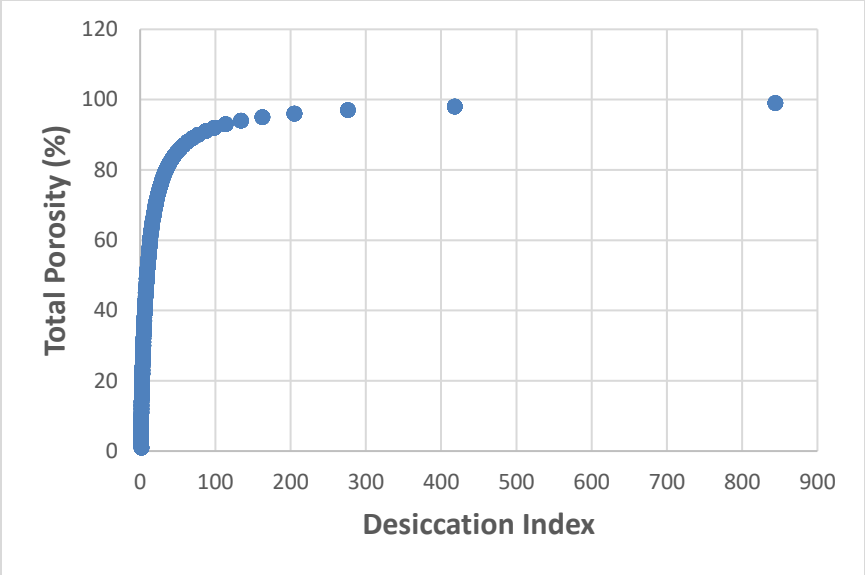

Figure 43: Monte Carlo, varied porosity all other variables held to values listed in table 5.

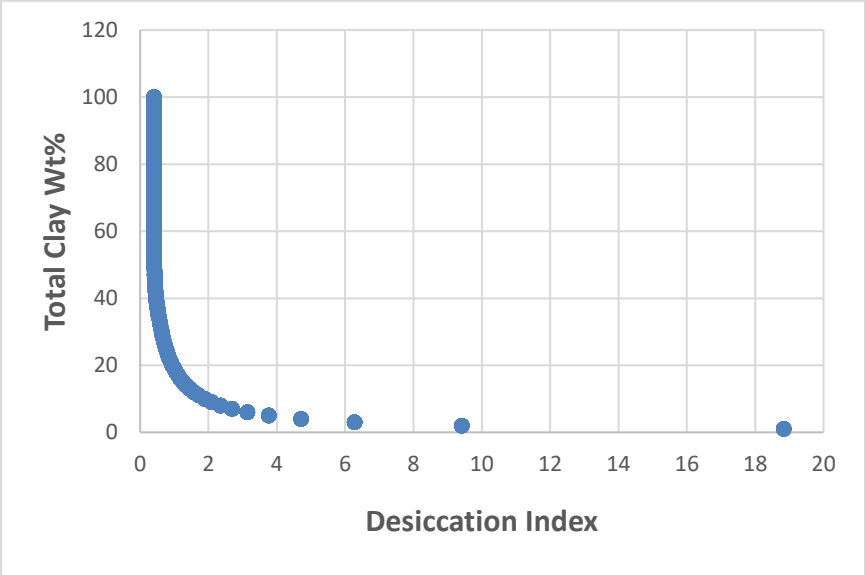

Figure 44: Monte Carlo, varied total weight percent clay, all other values held to variables in table 5.

Total porosity is permitted to vary between 0 and 100 percent in increments of 1%; the model failed to produce an estimation for porosities less than 1% and greater than 99% (Figure 43). This model results in a smooth curve with a minimum DI value of 0.79 at 3% total porosity and a maximum DI value of 844.3 at 99% porosity. Porosity and DI have a negative correlation. Larger porosity values correspond to larger DI values, maintaining an approximately linear trend between 3 - 70 %, after this point, it deviates sharply into very large DI values.

Total clay is varied between 0 and 100% in steps of 1% (Figure 44). The model failed to produce a prediction at 0% clay. At 100% clay, the model produced a DI value of 0.4, and at 1% clay, it produced a DI value of 18.83. This demonstrates that weight percent clay and DI have a negative association. There is an approximate linear association between 100 and 50% after this desiccation deviates sharply into large DI values.

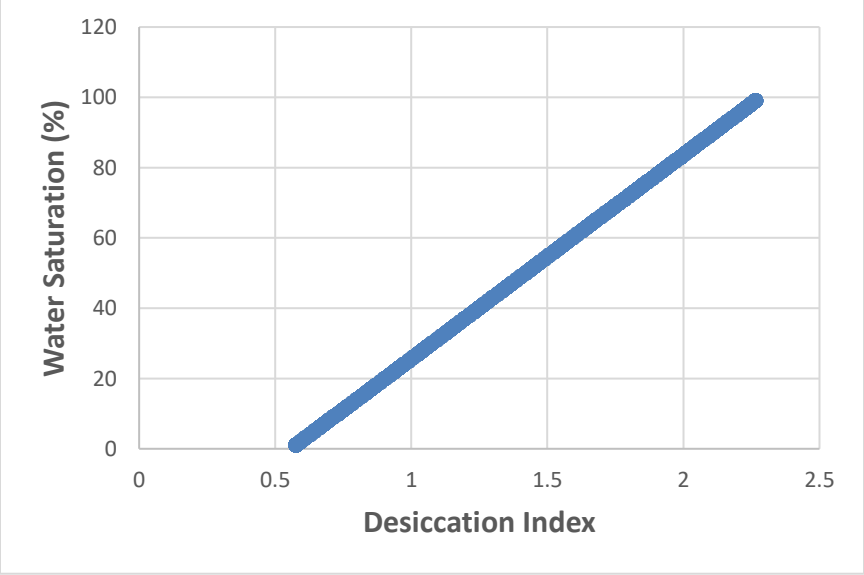

Figure 45: Monte Carlo, varied water saturation all other variables in table 5.

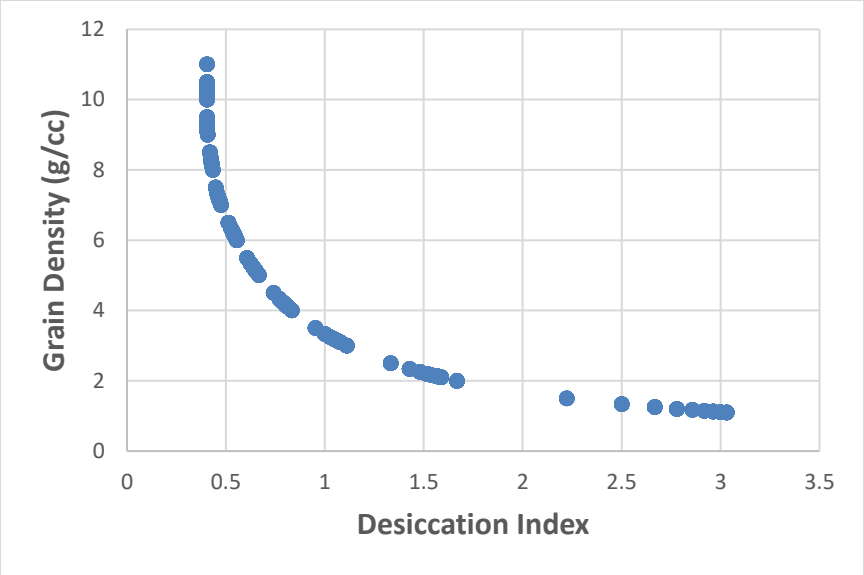

Figure 46: Monte Carlo, varied grain density all other variables held to values in table 5.

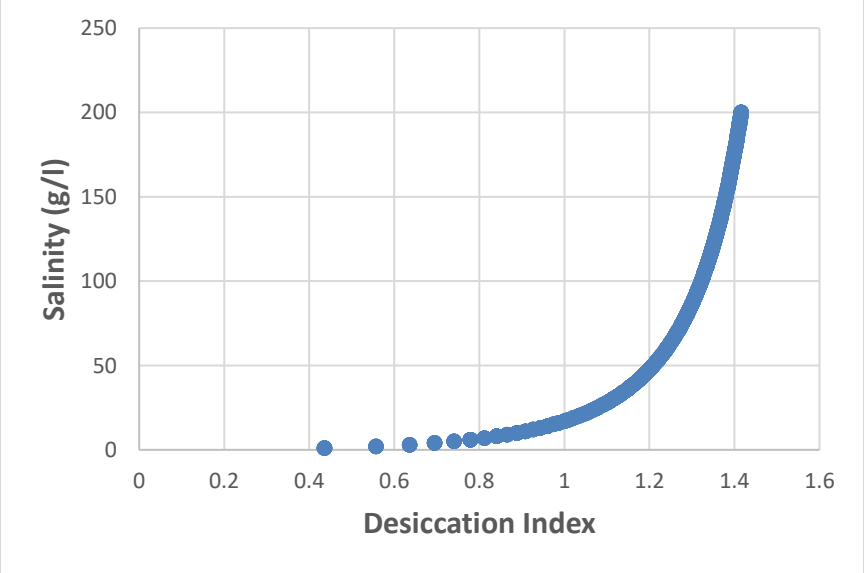

Figure 47: Monte Carlo, varied salinity all other variables held to values in table 5.

Water saturation is varied between 0 and 100% in increments of 1% (Figure 45). Calculated desiccation with zero water saturation was 0.576 and 2.265 at 100% water saturation. The plot shows a positive and linear association between water saturation and DI.

Grain density is varied between 1 and 11 g/cc in increments of 0.1 g/cc. Calculated desiccation at 11 g/cc was 0.4 and 3.03 at 1g/cc (Figure 46). The plot shows a negative non-linear association between grain density and DI, the produced plot having a slight curve with higher grain density values being associated with lower DI values.

Salinity is varied between 0 and 200 g/L in increments of 1 g/L (Figure 47). Calculated desiccation at salinity at 0 g/L was 0.43 and 1.42 at 200 g/L. The association between salinity and DI is positive and non-linear, as salinity values increase DI values sharply increase.

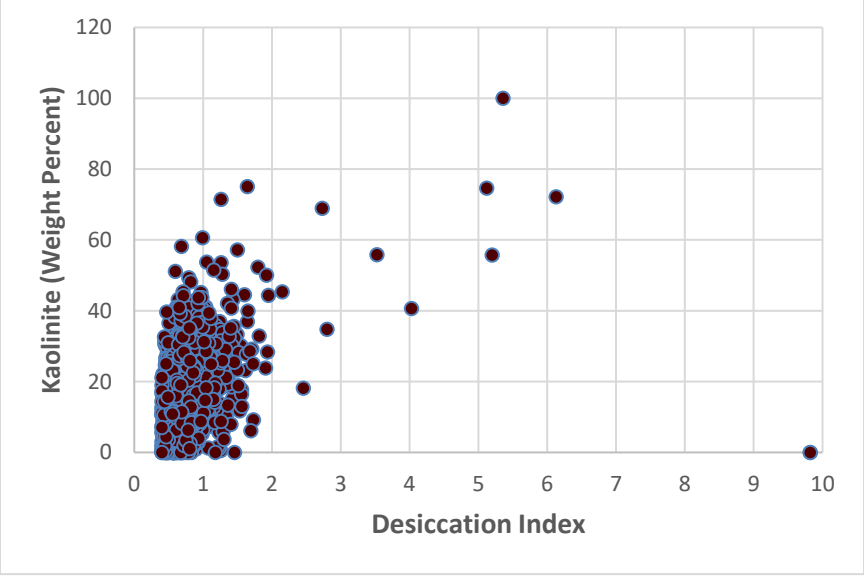

Figure 48: Monte Carlo, kaolinite, clay species weight percentages varied all other variables held to values in table 5.

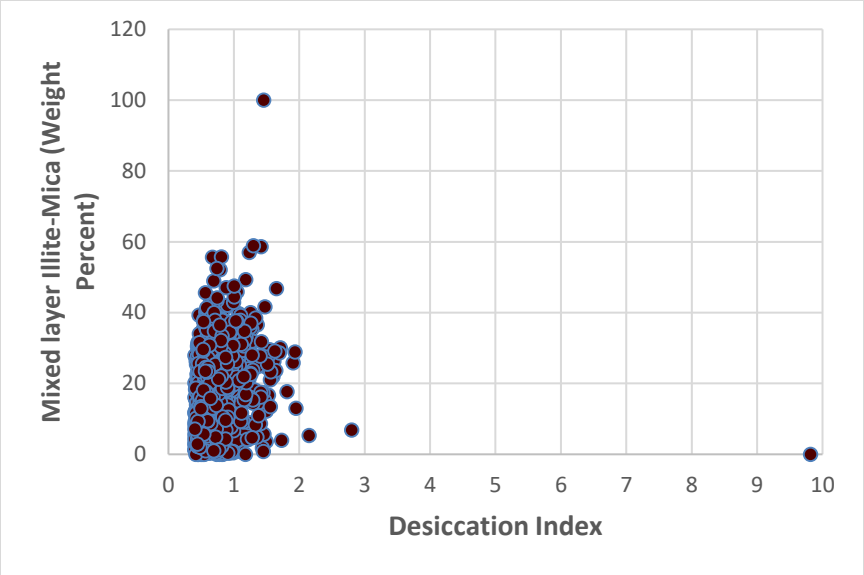

Figure 49: Monte Carlo, mixed layer illite-mica, clay species weight percentages varied all other variables held to values in table 5.

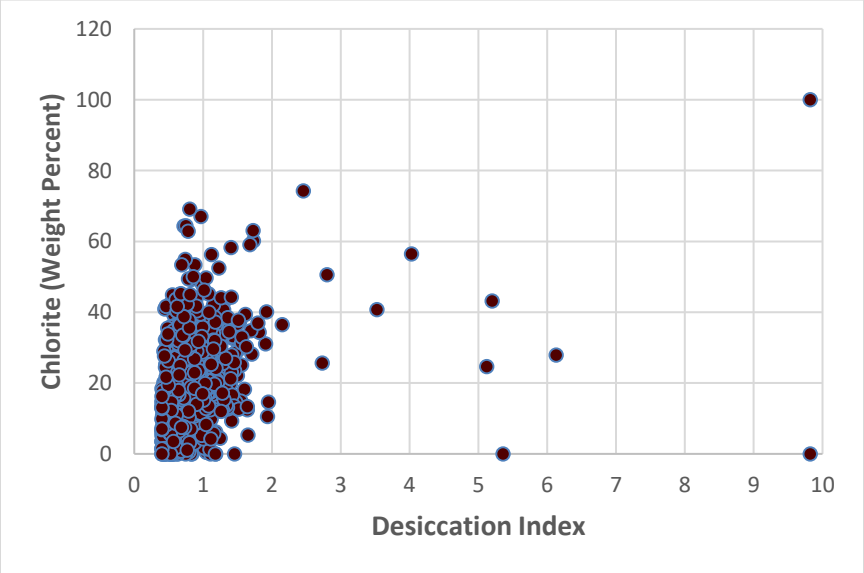

Figure 50: Monte Carlo, chlorite, clay species weight percentages varied all other variables held to values in table 5.

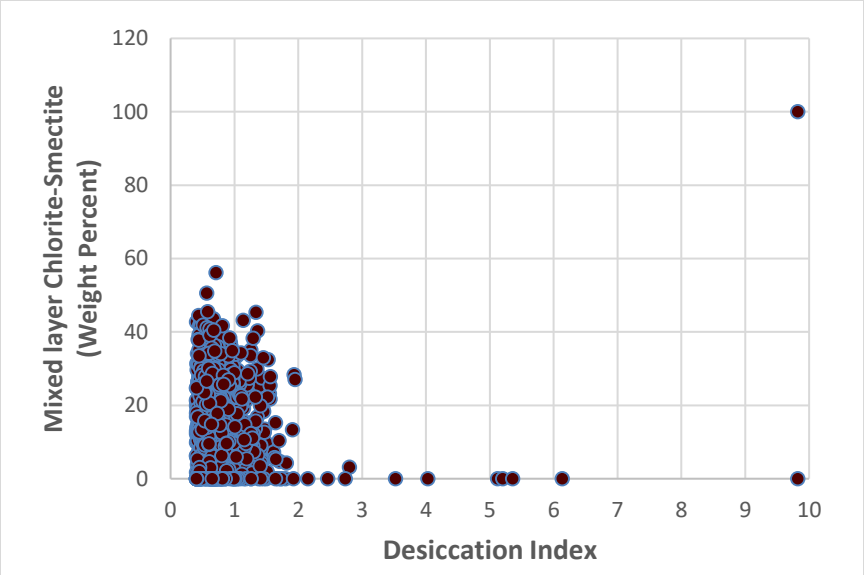

Figure 51: Monte Carlo, mixed layer chlorite-smectite, clay species weight percentages varied all other variables held to values in table 5.

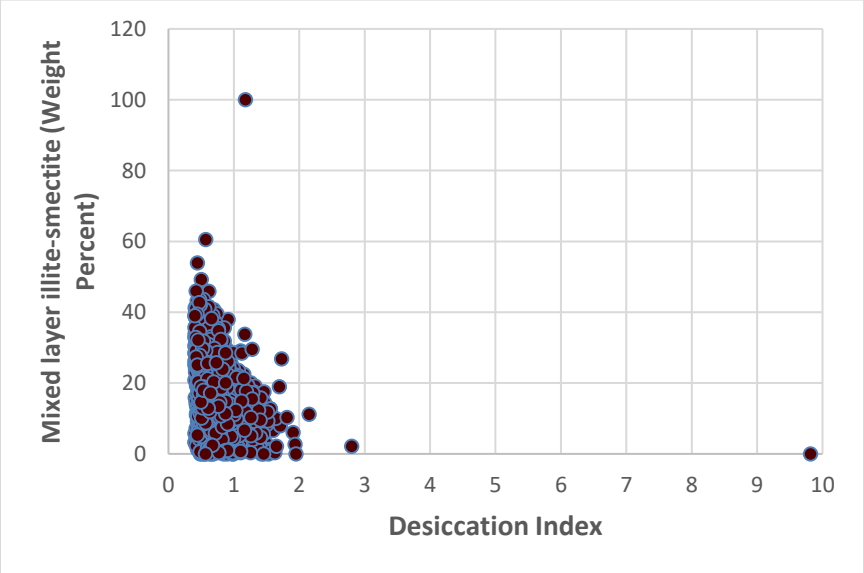

Figure 52: Monte Carlo, mixed layer illite-smectite, clay species weight percentages varied all other variables held to values in table 5.

Varying the weight percent of clay species while holding non-clay factors to constants produced significant scatter in all cases (Figure 48, Figure 49; Figure 50, Figure 51, Figure 52). The lowest DI value is 0.4 and was achieved in all clay species variance cases, the largest DI value is 9.81 and is achieved in the cases of 100% chlorite.

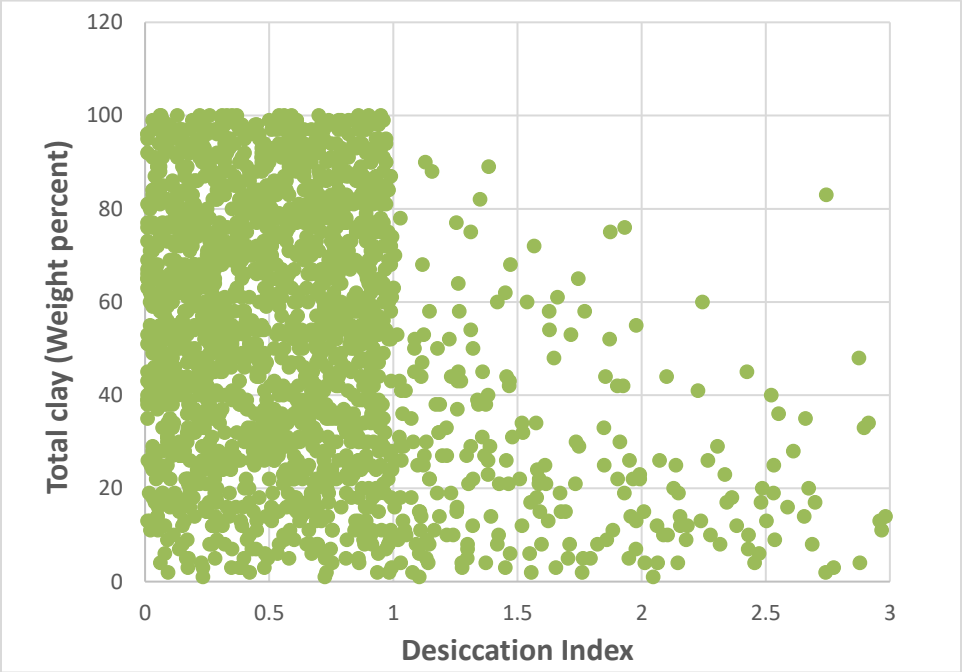

Figure 53: Monte Carlo, total clay all variables randomized.

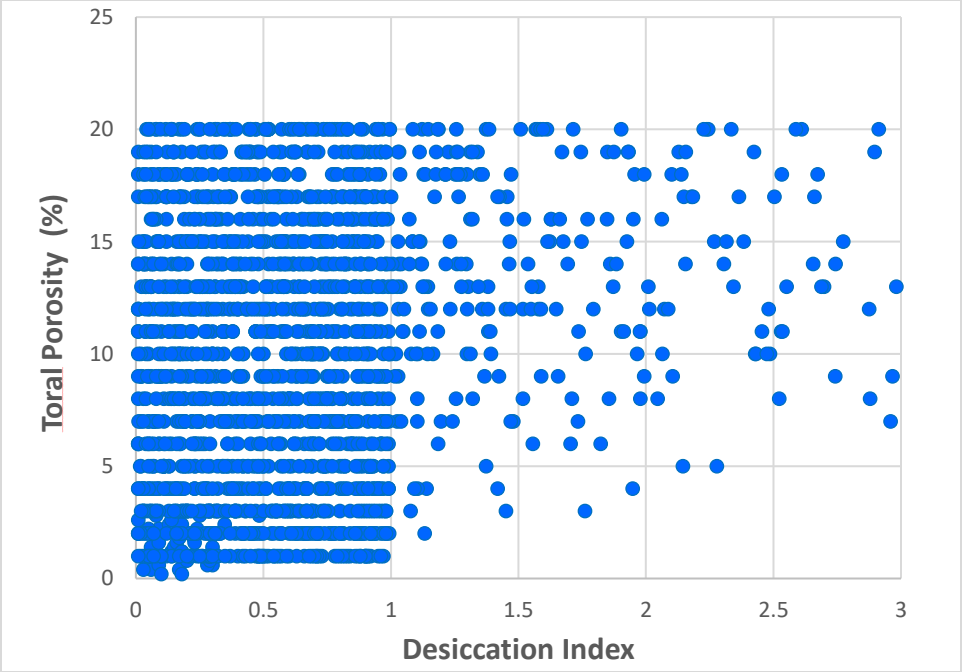

Figure 54: Monte Carlo, total porosity, all variable randomized.

Next, all factors are varied between endmember values. Grain density is varied between 0 – 5 g/cc, total porosity is varied between 0 – 20 %, water saturation and weight percent clay are varied between, and 0 -100% respectively. Salinity held at 98.437 g/L (the average of high and low pore fluid salinity estimations). Individual clay species are permitted to vary between 0 and 100%, however, their plots produced total scatter. Clay vs DI have significant scatter; however, data points tend to cluster at DI values less than 1 with increasing clay values (Figure 53). Inversely, when comparing total porosity and DI, there is greater clustering at DI values less than 1 with lower porosity values (Figure 54). DI values have a negative association with grain density, producing less scatter tat DI values less than one (Figure 55). Water saturation maintains

a strong positive association with DI despite variable randomization. There is a sharp linear cutoff of scattering towards lower DI values following the trend of $y = x\left(\frac{.98}{98}\right)$ (Figure 56).

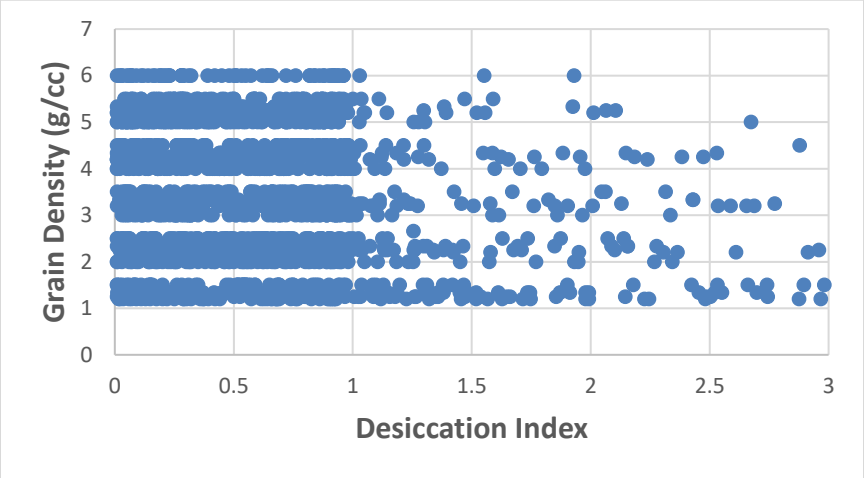

Figure 55: Monte Carlo, grain density, all variables randomized.

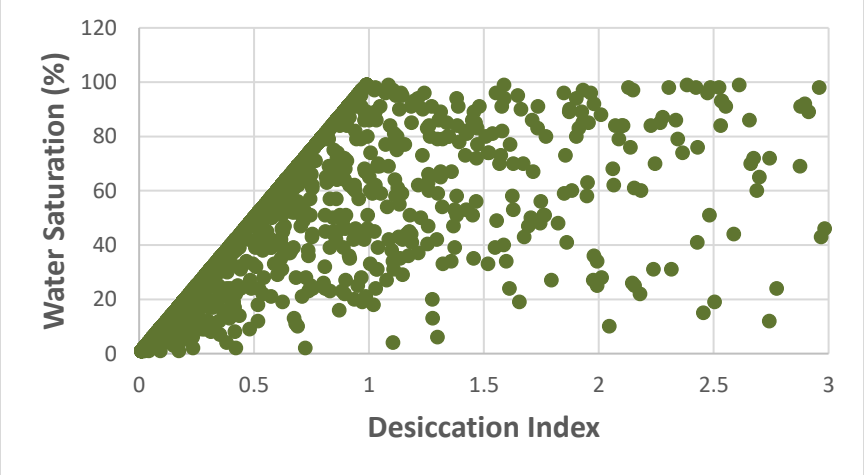

Figure 56: Monte Carlo, total water saturation, all variables randomized.

The results of the Monte Carlo investigation suggest that the largest changes in final desiccation value come from changes in clay content and porosity. Clay content is a major factor in rock CEC and directly affects the total grain density. Total porosity affects the volume of space in the rock for fluids and clays to occupy, this affects the volume of water necessary to displace to achieve desiccation. Total porosity also affects the total surface area of clays exposed to open pore space, influencing the number of binding locations.

CHAPTER 4

CONCLUSIONS

Monte Carlo simulation and analysis of core data concludes that the most significant rock properties for sediment dewatering are total porosity and total clay content. Changes in total porosity and total clay result in the largest changes in DI, as they most directly impact the capacity of the rock to hold water. Changes in other rock properties produce relatively minor variations. Additionally, rocks with higher degrees of organic richness are associated with lower DI values. Rocks with greater present-day organic richness may actively displace water in the pore system. Those with lower organic richness may not actively produce enough volumes of hydrocarbons to displace water, which permits rehydration if a desiccated state was achieved. The use of cobalt hexamine trichloride and ICP-MS in CEC measurement presents a rapid and cost-effective solution for precise characterization of rock clay properties. Corrections for sample grinding increase the utility of measured CEC for subsurface geoscience as they provide an accurate picture of subsurface rocks water capacity. Calculating grinding corrections from two data points instead of three is not recommended but does not result in widely different values. One must consult the correction slope and trends in the other measured data first before using two datapoints. When utilizing ICP-MS, the data collection plan must account for the differing dilutions required for the analysis of exchangeable cations and saturating solution. Elements measured by XRF and multivariable linear regressions present efficient means of generating accurate CEC estimations as densely as desired. Furthermore, the statistical assembly of the CEC regression formula provides an image of the interaction between clays, organics, and

composition of the pore fluid. XRF regression models for CEC present means of generating accurate and high-resolution reservoir characterizations.

REFERENCES

1. Alvarez, J. O., Tovar, F. D., & Schechter, D. S. (2017, September). Improving Oil Recovery in Unconventional Liquid Reservoirs by Soaking-Flowback Production Schedule with Surfactant Additives. *In SPE Liquids-Rich Basins Conference-North America*. Society of Petroleum Engineers.
2. Bernard, E., Lothenbach, B., Cau-Dit-Coumes, C., Chlique, C., Dauzères, A., & Pochard, I. (2018). Magnesium and calcium silicate hydrates, Part I: Investigation of the possible magnesium incorporation in calcium silicate hydrate (CSH) and of the calcium in magnesium silicate hydrate (MSH). *Applied geochemistry*, *89*, 229-242.
3. Bostrom, N., Chertov, M., Pagels, M., Willberg, D., Chertova, A., Davis, M., & Zagorski, W. (2014, February). The time-dependent permeability damage caused by fracture fluid. *In SPE International Symposium and Exhibition on Formation Damage Control*. Society of Petroleum Engineers.
4. Burst, J. F. (1976). Argillaceous sediment dewatering. *Annual Review of Earth and Planetary Sciences*, 4(1), 293-318.
5. Bush, D. C., & Jenkins, R. E. (1977, January). CEC determinations by correlations with adsorbed water. *In SPWLA 18th Annual Logging Symposium*. Society of Petrophysicists and Well-Log Analysts.
6. Ciesielski, H., Sterckeman, T., Santerne, M., & Willery, J. P. (1997). A comparison between three methods for the determination of cation exchange capacity and exchangeable cations in soils.

7. Chakraborty, N., & Karpyn, Z. T. (2015, September). Gas Permeability Evolution with Soaking Time in Ultra Tight Shales. *In SPE Annual Technical Conference and Exhibition*. Society of Petroleum Engineers.
8. Ciesielski, H., Sterckeman, T., Santerne, M., & Willery, J. P. (1997). A comparison between three methods for the determination of cation exchange capacity and exchangeable cations in soils.
9. Dessouki, M., Myers, M. T., Hathon, L. A., & Lee, J. M. (2016, June). The Influence of CEC, Salinity, and Silt Content on the Stress Dependent Petrophysical Properties of Resedimented Mudrocks. *In 50th US Rock Mechanics/Geomechanics Symposium*. American Rock Mechanics Association.
10. Dixon, J. B., & Schulze, D. G. (2002). *Soil mineralogy with environmental applications*. Soil Science Society of America Inc.
11. Dubois, I. E. (2011). Specific surface area of some minerals commonly found in granite (Licentiate dissertation). KTH Royal Institute of Technology, Stockholm. Retrieved from http://urn.kb.se/resolve?urn=urn:nbn:se:kth:diva-41259
12. Durand, C., Cerepi, A., & Brosse, E. (2000, January). Effect of pore-lining chlorite on petrophysical properties of low-resistivity sandstone reservoir. In *SPE Annual Technical Conference and Exhibition*. Society of Petroleum Engineers.
13. Dutta, R., Lee, C. H., Odumabo, S., Ye, P., Walker, S. C., Karpyn, Z. T., . & Luis, F. (2014). Experimental investigation of fracturing-fluid migration caused by spontaneous imbibition in fractured low-permeability sands. *SPE Reservoir Evaluation & Engineering*, 17(01), 74-81.

14. Engelder, T., Cathles, L. M., & Bryndzia, L. T. (2014). The fate of residual treatment water in gas shale. *Journal of Unconventional Oil and Gas Resources,* 7, 33-48.
15. Hill, H. J., Klein, G. E., Shirley, O. J., Thomas, E. C., & Waxman, W. H. (1979). Bound water in shaly sands-its relation to Q and other formation properties. *The log analyst*, *20*(03).
16. Huff, G. F. (1987). A correction for the effect of comminution on the cation exchange capacity of clay-poor sandstones. *SPE Formation Evaluation,* 2(03), 338-344.
17. Lan, Q., Ghanbari, E., & Dehghanpour, H. (2014, February). Water loss versus soaking time: spontaneous imbibition in tight rocks. In *SPE/EAGE European Unconventional Resources Conference and Exhibition.*
18. Martin, P., & Dacy, J. (2004, January). Effective Qv by NMR core tests. In *SPWLA 45th Annual Logging Symposium*. Society of Petrophysicists and Well-Log Analysts.
19. Macht, F., Eusterhues, K., Pronk, G. J., & Totsche, K. U. (2011). Specific surface area of clay minerals: Comparison between atomic force microscopy measurements and bulk-gas (N2) and-liquid (EGME) adsorption methods. *Applied Clay Science*, *53*(1), 20-26.
20. Pollastro, R. M. (1990). The illite/smectite geothermometer—concepts, methodology, and application to basin history and hydrocarbon generation. Rocky Mountain Section (SEPM).
21. Sánchez-Martín, M. J., Dorado, M. C., Del Hoyo, C., & Rodríguez-Cruz, M. S. (2008). Influence of clay mineral structure and surfactant nature on the adsorption capacity of surfactants by clays. *Journal of Hazardous Materials*, *150*(1), 115-123.

22. Sharma, A., Weindorf, D. C., Wang, D., & Chakraborty, S. (2015). Characterizing soils via portable X-ray fluorescence spectrometer: 4. Cation exchange capacity (CEC). *Geoderma*, *239*, 130-134.

23. Sharma, A., Weindorf, D. C., Man, T., Aldabaa, A. A. A., & Chakraborty, S. (2014). Characterizing soils via portable X-ray fluorescence spectrometer: 3. Soil reaction (pH). *Geoderma*, *232*, 141-147.

24. Tissot, B. P., & Welte, D. H. (1984). Petroleum Formation and Occurrence, 2nd edn, 699 pp.

25. Waxman, M. H., & Smits, L. J. M. (1968). Electrical conductivities in oil-bearing shaly sands. *Society of Petroleum Engineers Journal*, 8(02), 107-122.

26. Waxman, M. H., & Thomas, E. C. (1974). Electrical conductivities in shaly sands–II. The temperature coefficient of electrical conductivity. *J. Petrol. Technol. Trans. AIME*, 257, 218.

27. Yaich, E., Williams, S., Goddard, P., de Souza, O. D., Bowser, A., & Foster, R. A. (2015, July). A case study: The impact of soaking on well performance in the Marcellus. In *Unconventional Resources Technology Conference*, San Antonio, Texas, 20-22 July 2015 (pp. 1911-1920). Society of Exploration Geophysicists, American Association of Petroleum Geologists, Society of Petroleum Engineers.

28. Yu, Y., Li, L., & Sheng, J. J. (2016, September). Further discuss the roles of soaking time and pressure depletion rate in gas huff-n-puff process in fractured liquid-rich shale reservoirs. In *SPE Annual Technical Conference and Exhibition*. Society of Petroleum Engineers.

29. Jacobs, T. (2017). Optimism and activity rising in the Vaca Muerta. Journal of Petroleum Technology, 69(05), 34-38.

30. Juhasz, I. (1979). The central role of Qv and formation-water salinity in the evaluation of shaly formations. *The Log Analyst*, *20*(04).

31. Jenni, A., Mäder, U., Lerouge, C., Gaboreau, S., & Schwyn, B. (2014). In situ interaction between different concretes and Opalinus Clay. *Physics and Chemistry of the Earth, Parts A/B/C*, *70*, 71-83.

32. Zhu, Y., Weindorf, D. C., & Zhang, W. (2011). Characterizing soils using a portable X-ray fluorescence spectrometer: 1. Soil texture. *Geoderma*, *167*, 167-177.

APPENDIX

The CEC contribution of illite is given by equation 7, which sums the CEC contributions of both mixed layer and discrete illite in the rock.

$$CEC_{Illite} = (Clay\ WT\% * IM * IM_I * CEC_{Illite\ Literature}) + (Clay\ WT\% * IM * IM_M * CEC_{Mica\ Literature}) + (Clay\ WT\% * IS * IS_I * CEC_{Illite\ Literature})$$

Equation 7: Statement for CEC of illite from XRD data (Dacy and Martin, 2004). IM: weight percent illite-mica mixed layer, IM_I: weight percent illite in illite-mica mixed layer, IM_M: weight percent mica in illite-mica mixed layer, IS: weight percent illite-smectite mixed layer, IS_I: weight percent illite in illite-smectite mixed layer.

The CEC contribution of kaolinite is given by equation 8.

$$CEC_{Kaolinite} = (Clay\ WT\% * K * CEC_{Kaolinite\ Literature})$$

Equation 8: Statement for CEC of illite from XRD data (Dacy and Martin, 2004). K: weight percent kaolinite.

The CEC contribution of chlorite is given by equation 9, which sums the CEC contributions of both mixed layer and discrete chlorite in the rock.

$$CEC_{Chlorite} = (Clay\ WT\% * C * CEC_{Chlorite\ Literature}) + (Clay\ WT\% * CS * CS_C * CEC_{Chlorite\ Literature})$$

Equation 9: Statement for CEC of illite from XRD data (Dacy and Martin, 2004). C: weight percent chlorite, CS_C: weight percent chlorite in chlorite-smectite mixed layer.

The CEC contribution of smectite is given by equation 10, which sums the CEC contributions of both mixed layer and discrete smectite in the rock.

$$CEC_{Smectite} = (Clay\ WT\% * S * CEC_{Smectite\ Literature}) + (Clay\ WT\% * CS * CS_S * CEC_{Smectite\ Literature}) + (Clay\ WT\% * IS * IS_S * CEC_{Literature})$$

Equation 10: Statement for CEC of illite from XRD data (Dacy and Martin, 2004). S: weight percent Smectite, CS_S: weight percent smectite in chlorite-smectite mixed layer.